Supplemental Materials

Table of Contents

1 Summary of the vibration testing models

In general, all considered nanowires (NWs) uniformly have a [110] longitudinal direction. Five orthogonal coordination systems have been established for the NW's cross-section, including C0: $[\bar{1}1\bar{2}]$ and $[\bar{1}11]$; C1: $[\bar{1}10]$ and [001]; C2: $[\bar{5}52]$ and $[1\bar{1}5]$; C3: $[\bar{3}32]$ and $[1\bar{1}3]$; and C4: $[\bar{5}56]$ and $[3\bar{3}5]$. During each simulation, either the velocity actuation or the displacement actuation is applied. Both approaches increase the total potential energy of the atomic system by less than 0.1% to secure that nonlinear vibration modes haven't been excited. The examined models have been categorized into thirteen groups according to the appearance sequence in the paper, as listed below.

Table I. Summary of the testing models (totally 66 cases).

Group No.	Total Case No.	Different NWs Material	Different NWs Cross-section	Factors
I	2	Ag	Circular	Consider actuation in either *x* or *y*-axis
II	4	Ag	Circular	Consider different cross-sectional sizes
III	4	Ag	Circular	Consider different actuation amplitudes
IV	4	Ag	Circular	Consider different temperatures
V	7	Ag	Circular	Consider different pre-strain values
VI	2	Ag	Square	Consider square cross-section
VII	2	Ag	Circular	Consider clamped-free boundary condition
VIII	5	Ag	Circular	Consider different temperatures under the displacement actuation
IX	8	Ag	Circular	Consider different actuation directions
X	12	Ag	—	Consider different cross-sectional geometries, i.e., pentagonal, rhombic and triangular
XI	1	Ag	Circular	Consider two simultaneous actuations
XII	5	—	Circular	Consider other [110] orientated FCC NWs, i.e., Au, Cu, Ni, Pd, Pt
XIII	10	Ag	Square	Consider different cross-sectional sizes

2 List of all numerical testing results

All testing results are listed below, including the time history of the external energy, as well as the corresponding frequency spectrum from fast Fourier transform analysis. For simplicity, following denotations are used, including:

- Coord. refers the coordination systems;
- Temp. refers the temperature;
- Å is the shortage of Angstrom;
- psec is the shortage picosecond;
- Vel. refers the velocity actuation;
- Disp. refers the displacement actuation;
- Size refers the NW's size, e.g., for circular cross-section: diameter×length.

2.1 Group I: 2 cases. Consider actuation in either *x* or *y*-axis

Setting: Circular Ag NWs; Size: 6×34.71 nm^2; Coord.: C0; Temp.: 10 K; Vel.: 0.8 Å/psec.

2.1.1 Actuation in x-axis

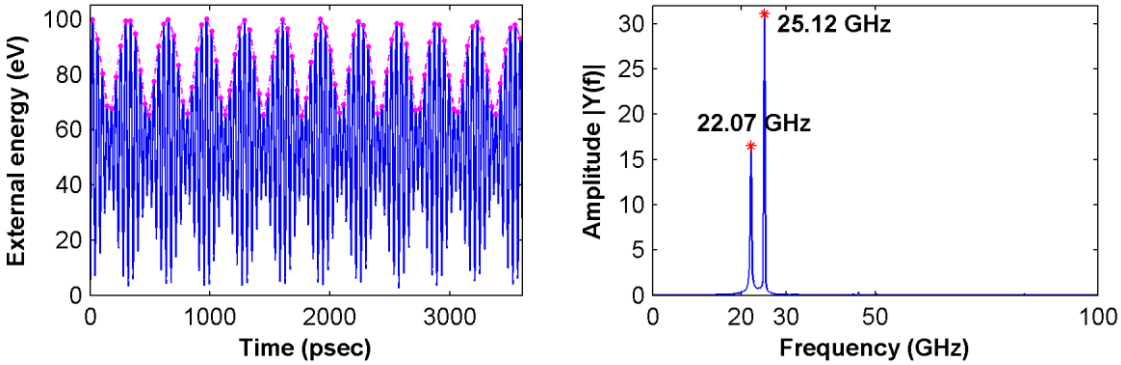

2.1.2 Actuation in y-axis

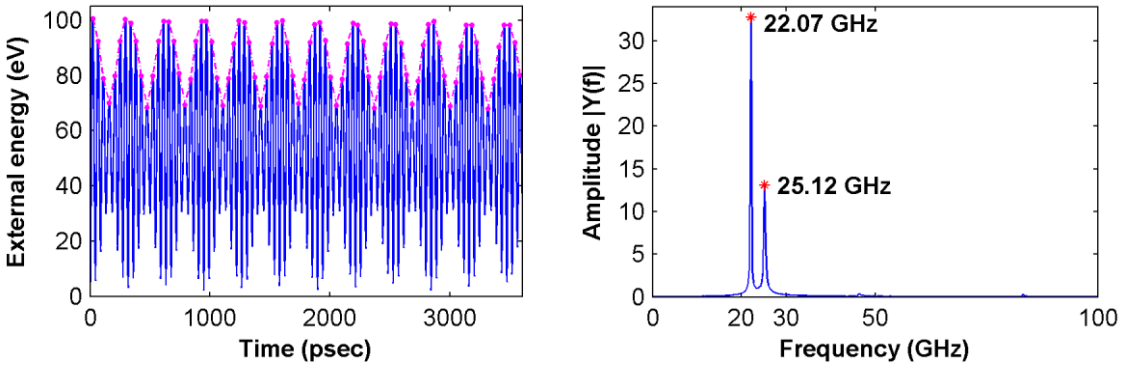

2.2 Group II: 4 cases. Consider different NW cross-section sizes

Setting: Circular Ag NWs, Coord.: C0; Temp.: 10 K; Vel.: *x*-axis

2.2.1 Size 4×34.71 nm^2, Vel.: 0.5 Å/psec

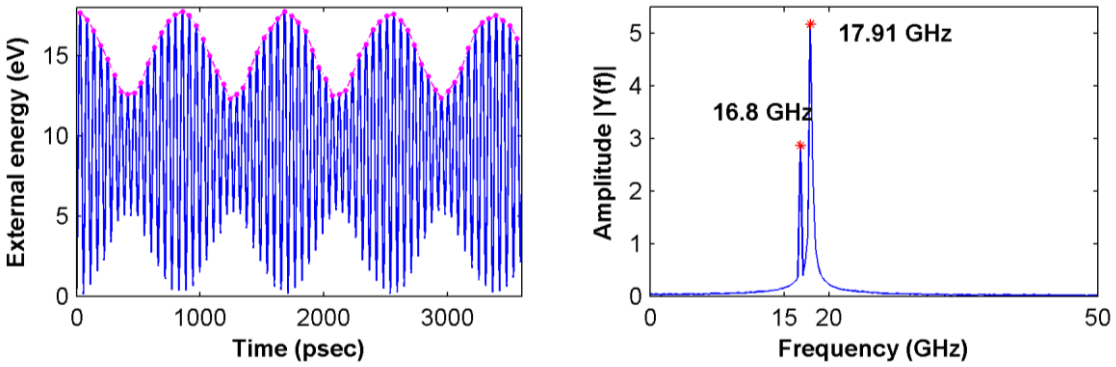

2.2.2 Size 5×34.71 nm^2, Vel.: 0.6 Å/psec

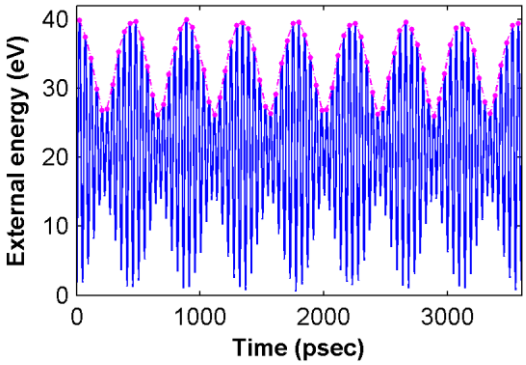

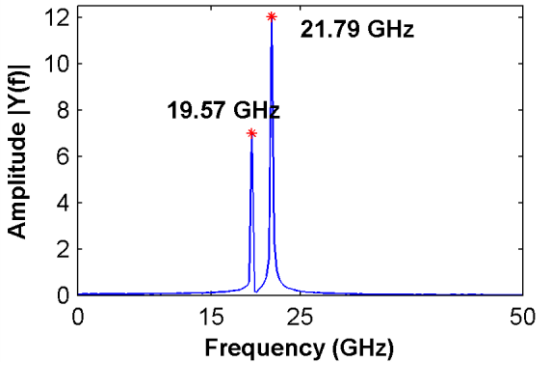

2.2.3 Size 7×34.71 nm^2, Vel.: 0.8 Å/psec

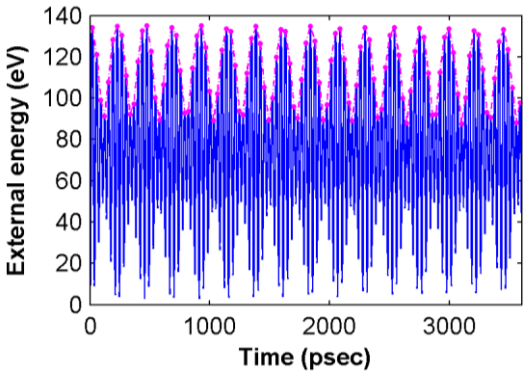

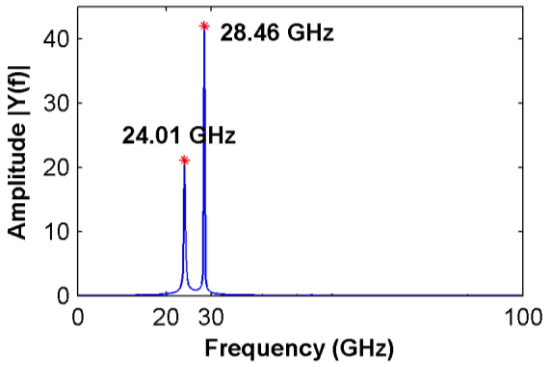

2.2.4 Size 8×34.71 nm^2, Vel.: 0.5 Å/psec

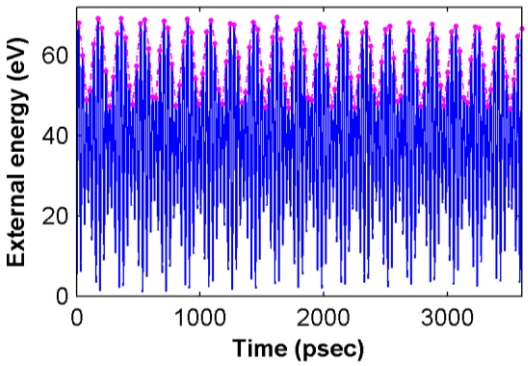

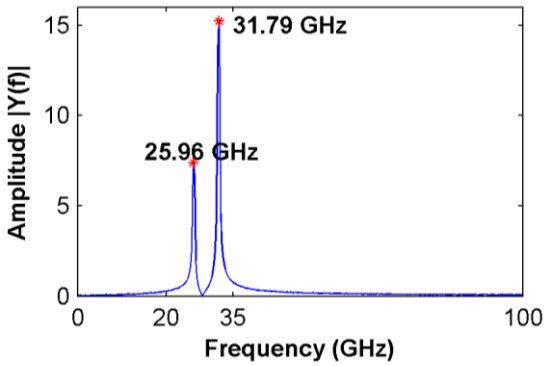

2.3 Group III: 4 cases. Consider different actuation amplitudes

Setting: Circular Ag NWs; Size: 6×34.71 nm^2; Coord.: C0; Temp.: 10 K; Vel.: *x*-axis

2.3.1 Actuation amplitude 0.6 Å/psec

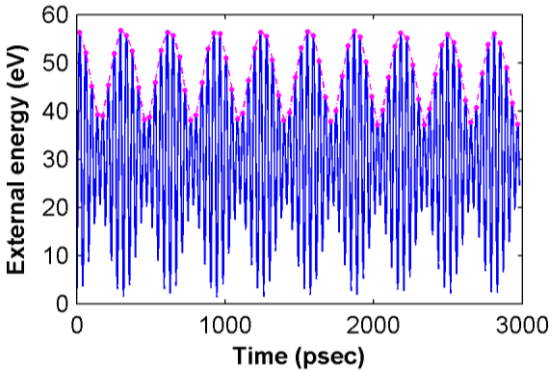

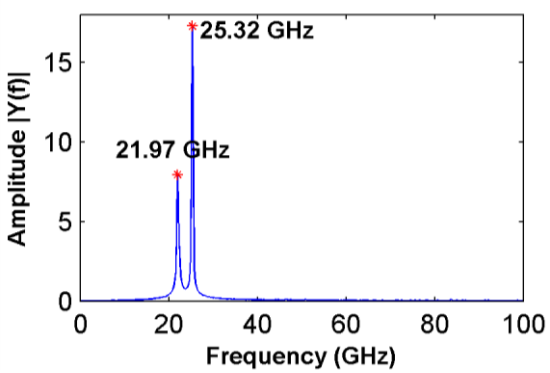

2.3.2 Actuation amplitude 0.4 Å/psec

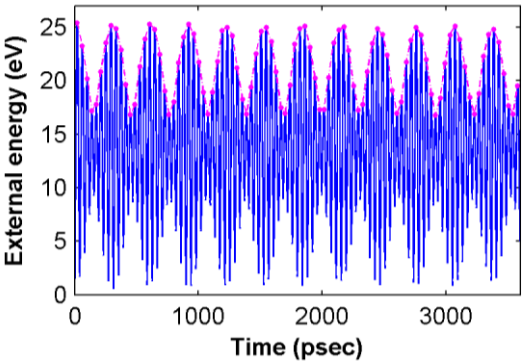

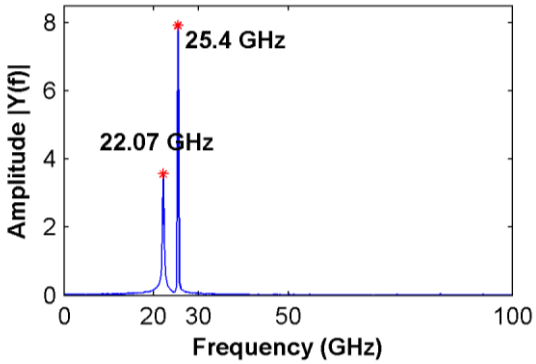

2.3.3 Actuation amplitude 0.2 Å/psec

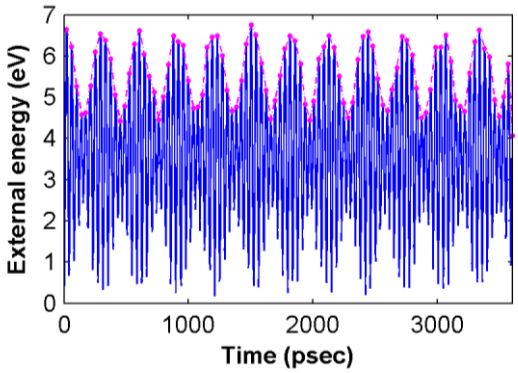

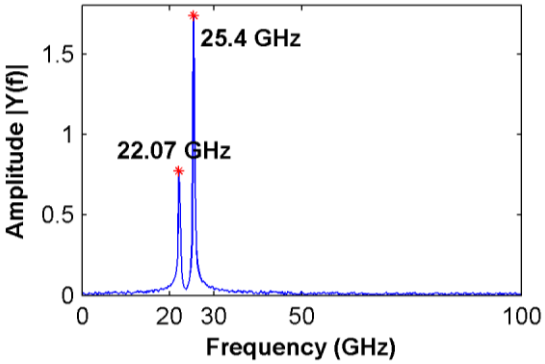

2.3.4 Actuation amplitude 0.1 Å/psec

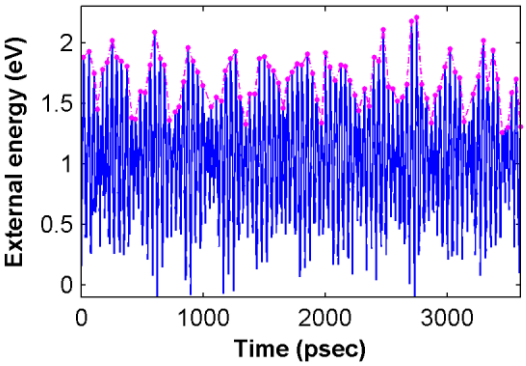

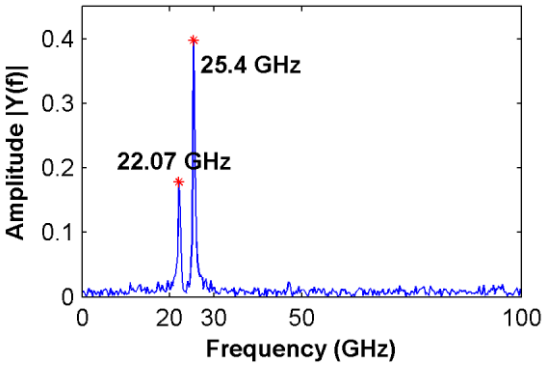

2.4 Group IV: 4 cases. Consider different temperatures

Setting: Circular Ag NWs; Size: 6×34.71 nm^2; Coord.: C0; Vel.: *x*-axis.

2.4.1 Temperature 0.1 K, Vel.: 0.8 Å/psec

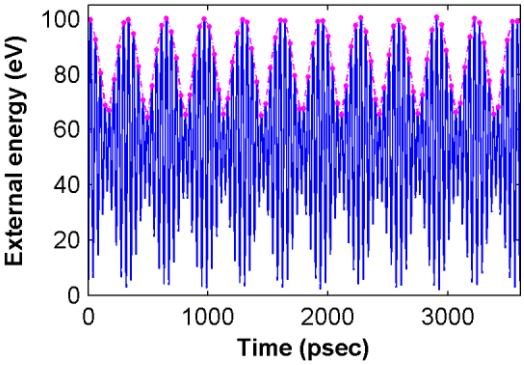

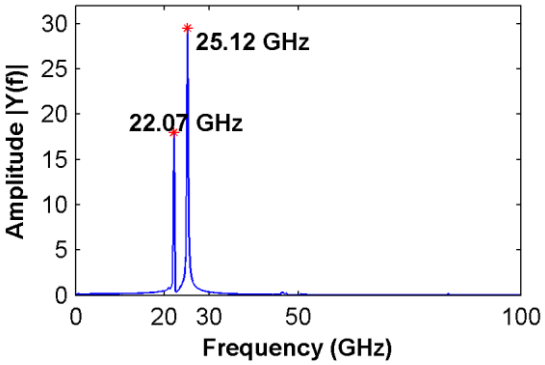

2.4.2 Temperature 100 K, Vel.: 0.8 Å/psec

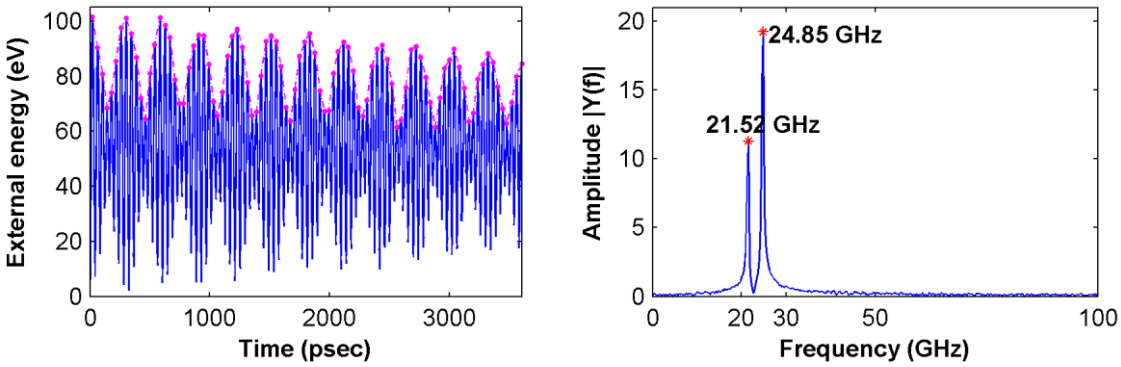

2.4.3 Temperature 200 K, Vel.: 0.8 Å/psec

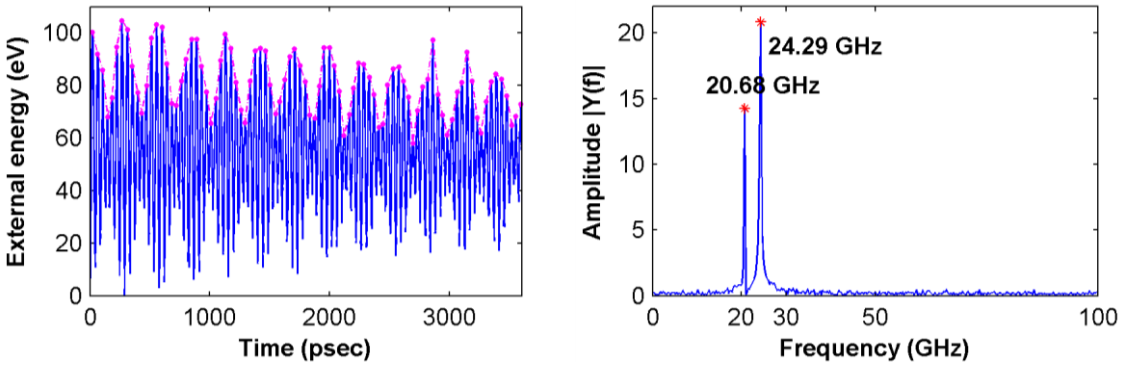

2.4.4 Temperature 300 K, Vel.: 0.8 Å/psec

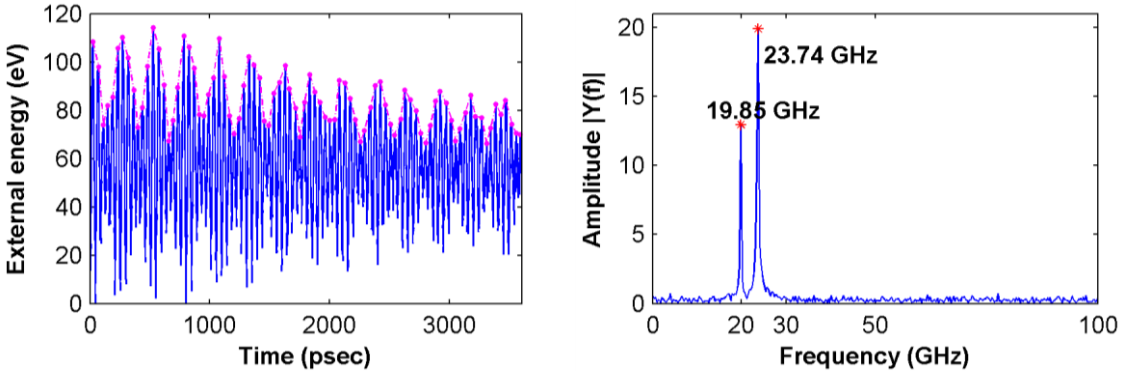

2.5 Group V: 7 cases. Consider different pre-strain values

Setting: Circular Ag NWs; Size: 6×34.71 nm^2; Coord.: C0; Temp.: 10 K; Vel.: *x*-axis.

2.5.1 Pre-tension 1.6%, Vel.: 0.1 Å/psec

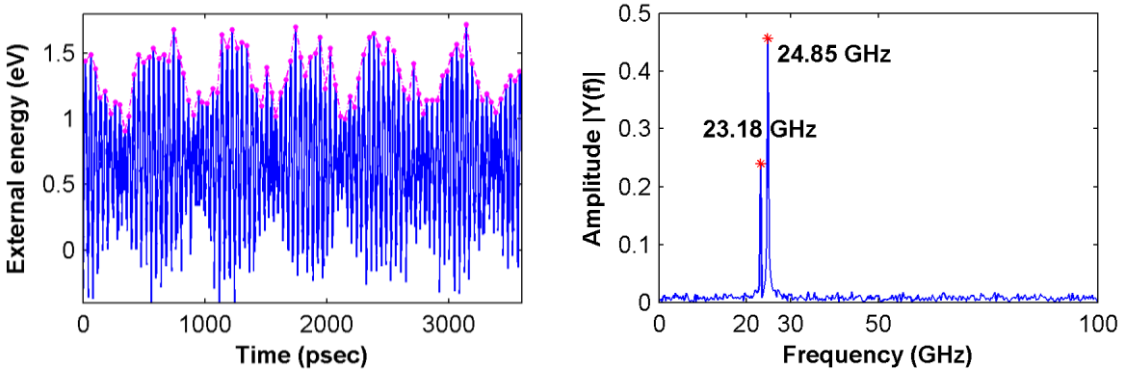

2.5.2 Pre-tension 2.67%, Vel.: 0.3 Å/psec

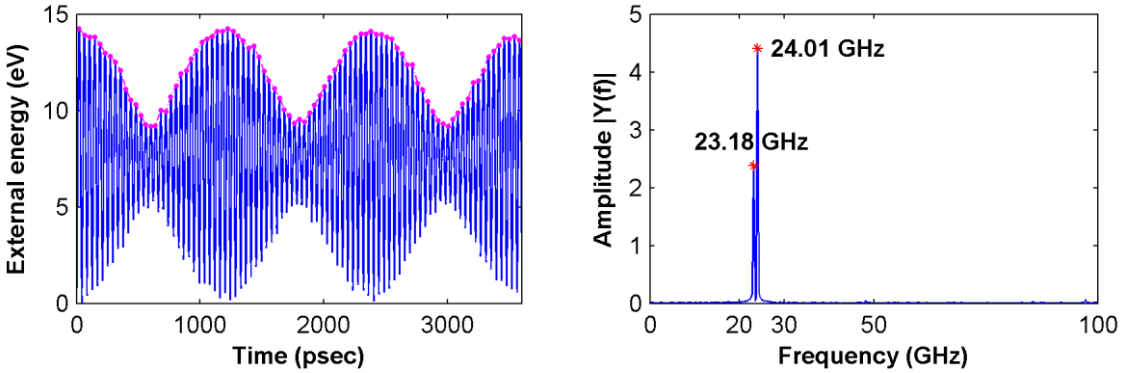

2.5.3 Pre-tension 3.48%, Vel.: 0.3 Å/psec

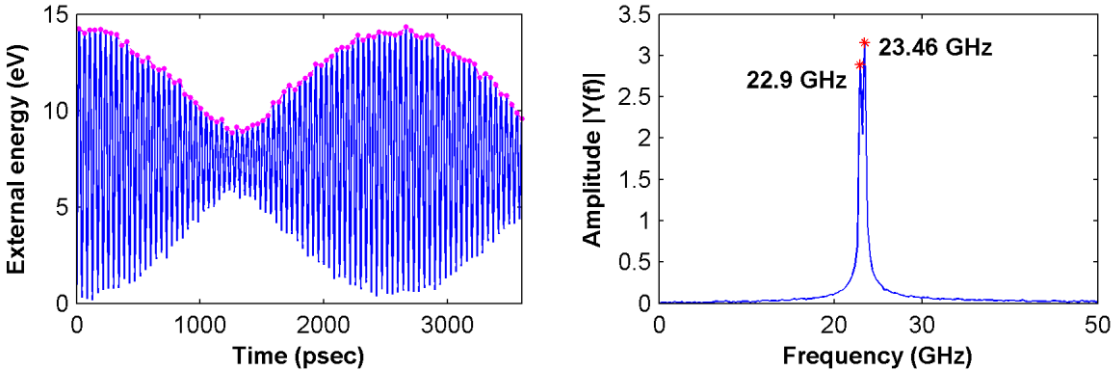

2.5.4 Pre-tension 4.81%, Vel.: 0.1 Å/psec

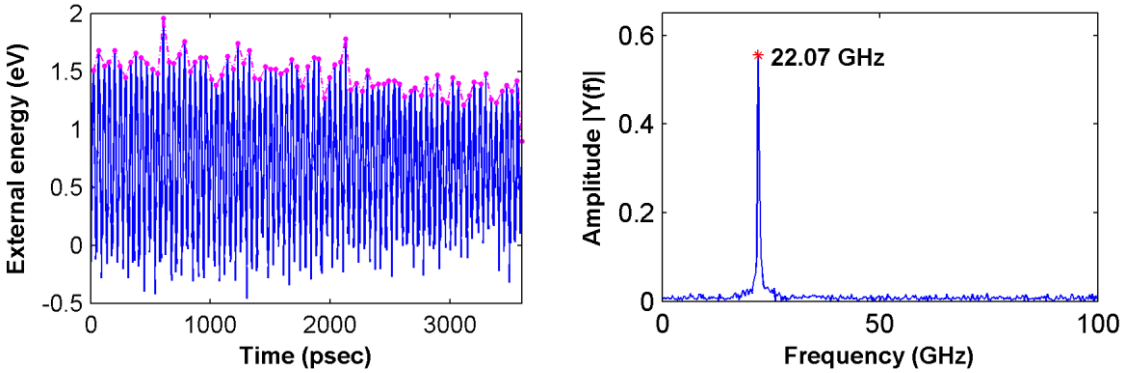

2.5.5 Pre-compression 1.6%, Vel.: 0.3 Å/psec

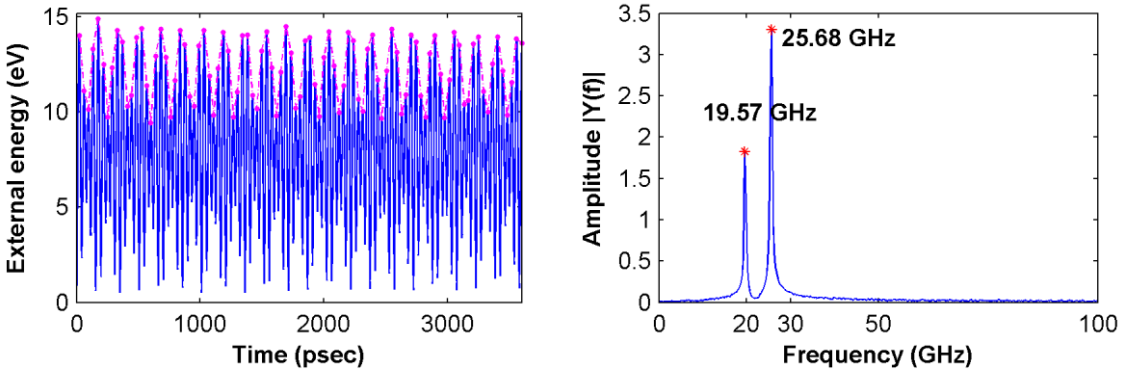

2.5.6 Pre-compression 2.67%, Vel.: 0.2 Å/psec

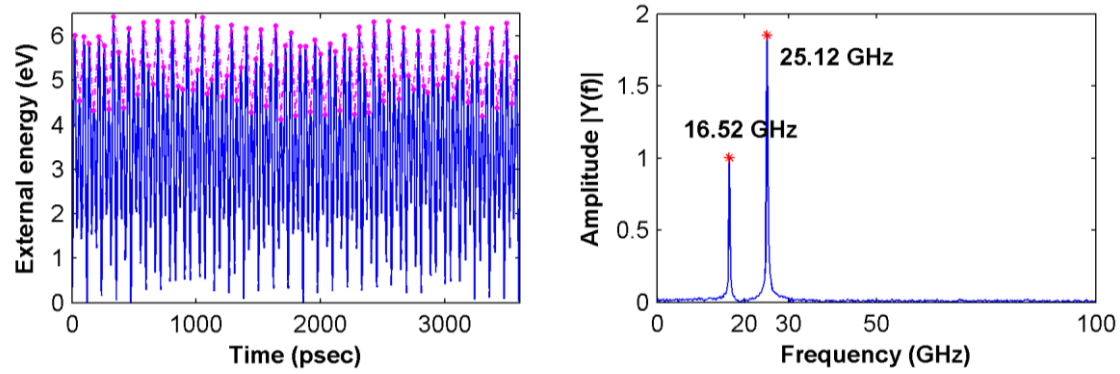

2.5.7 Pre-compression 3.48%, Vel.: 0.3 Å/psec

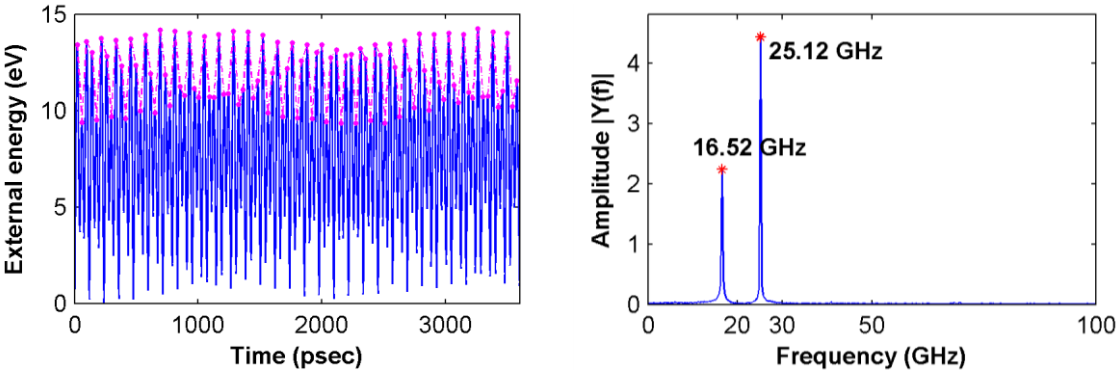

2.6 Group VI: 2 cases. Consider square cross-section

Setting: Square Ag NWs; Size: 3×24.87 nm^2; Coord.: C0; Temp.: 10 K; Vel.: 0.8 Å/psec.

2.6.1 Actuation in x-axis

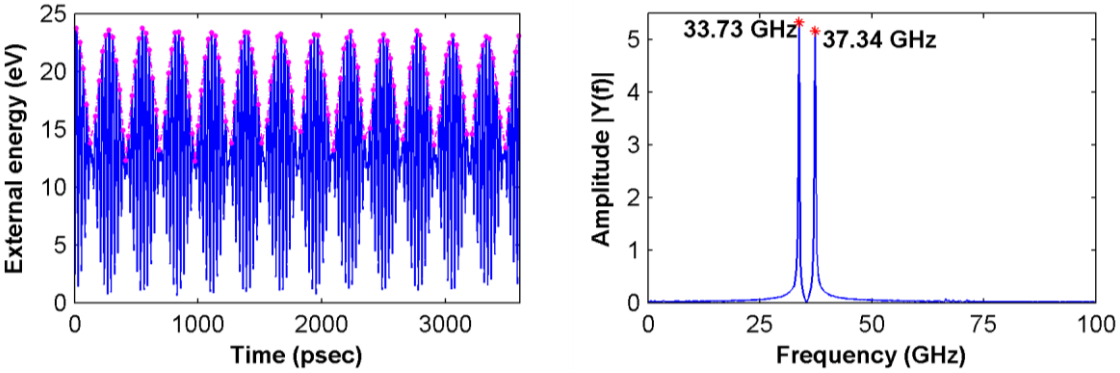

2.6.2 Actuation in y-axis

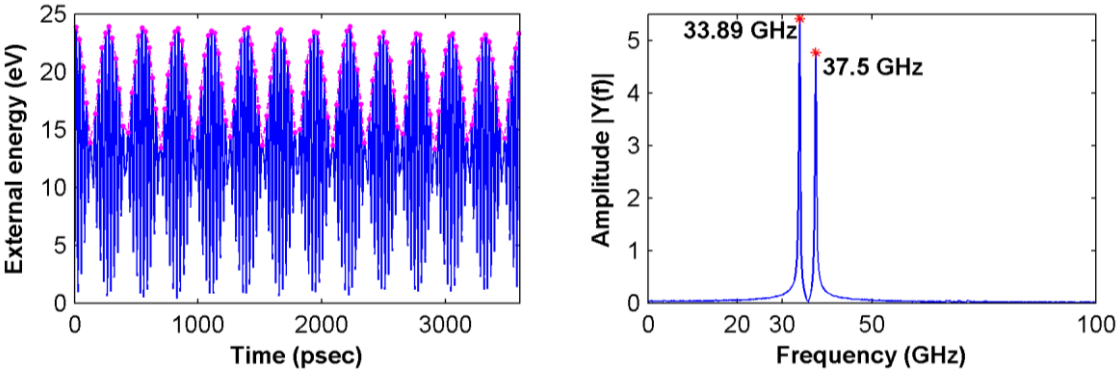

2.7 Group VII: 2 cases. Consider clamped-free boundary conditions

Setting: Clamped-Free, Circular Ag NWs; Size: 6×34.71 nm^2; Coord.: C0; Vel.: 0.2 Å/psec.

2.7.1 Actuation in x-axis

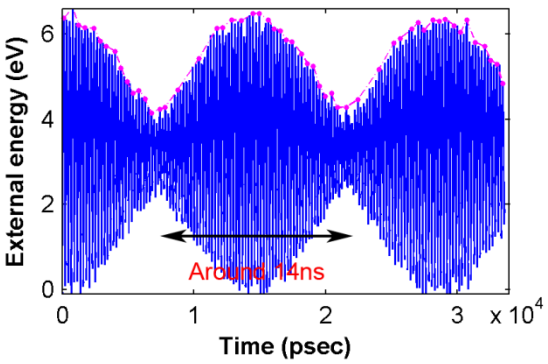

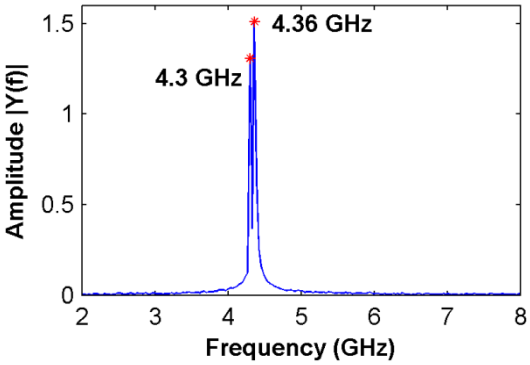

2.7.2 Actuation in y-axis

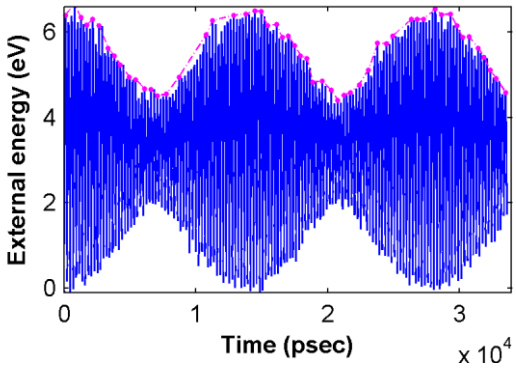

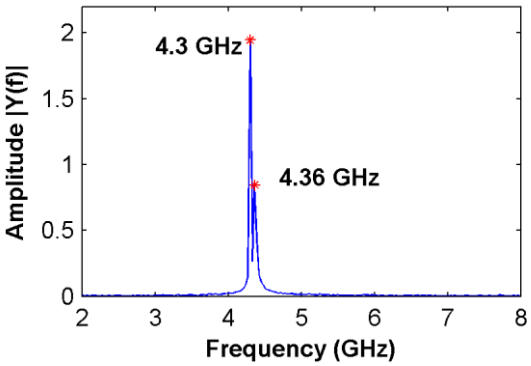

2.8 Group VIII: 5 cases. Consider different temperatures under displacement actuation

Setting: Circular Ag NWs; Size: 6×34.71 nm^2; Coord.: C0; Dis.: *x*-axis, 15 Å.

2.8.1 Temperature 0.1 K

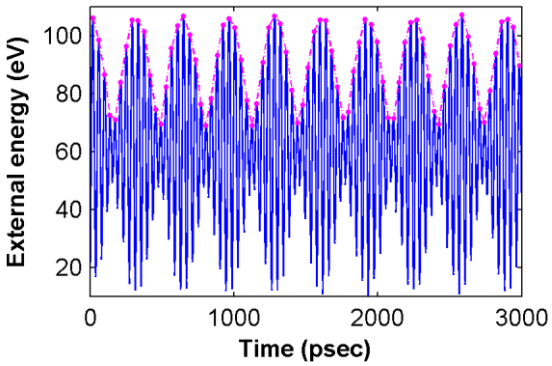

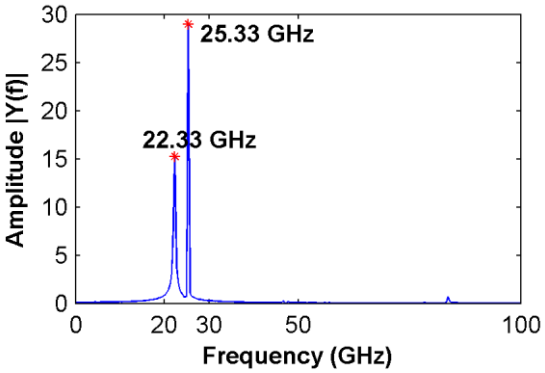

2.8.2 Temperature 10 K

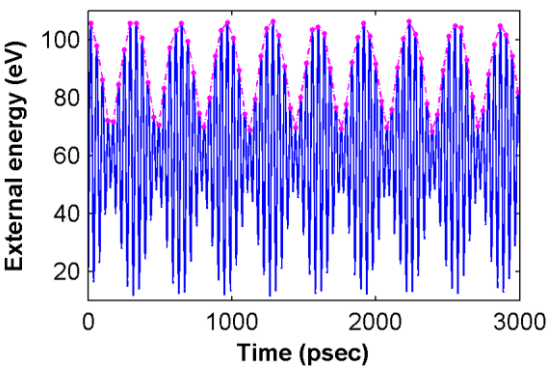

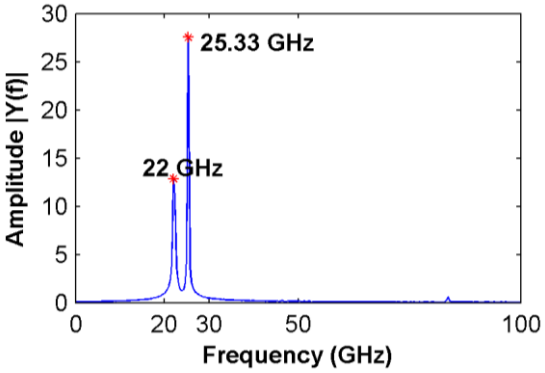

2.8.3 Temperature 100 K

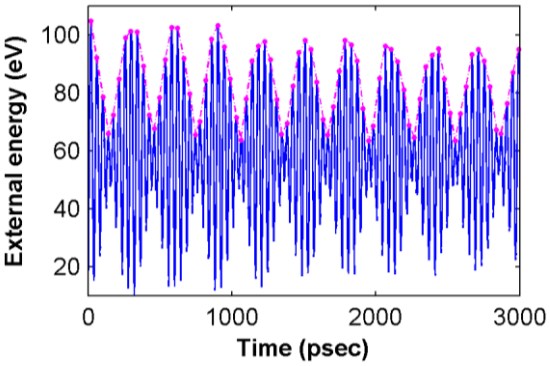

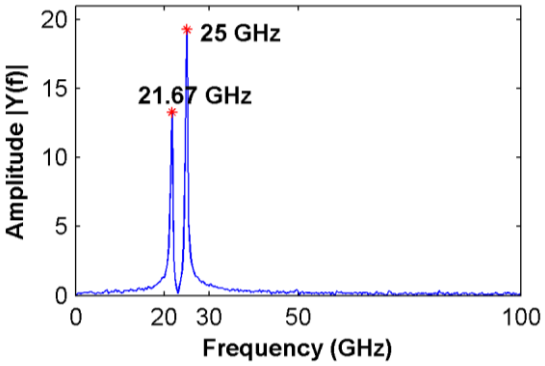

2.8.4 Temperature 200 K

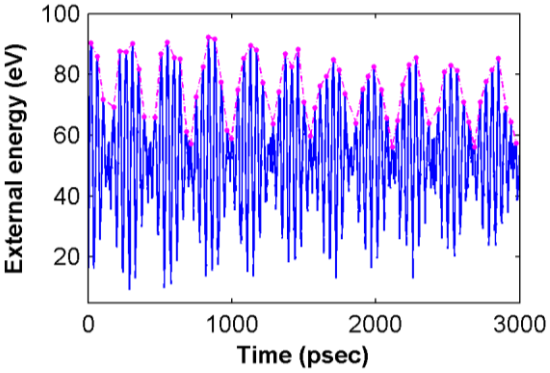

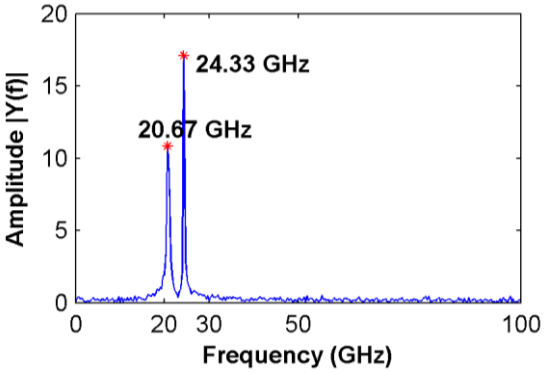

2.8.5 Temperature 300 K

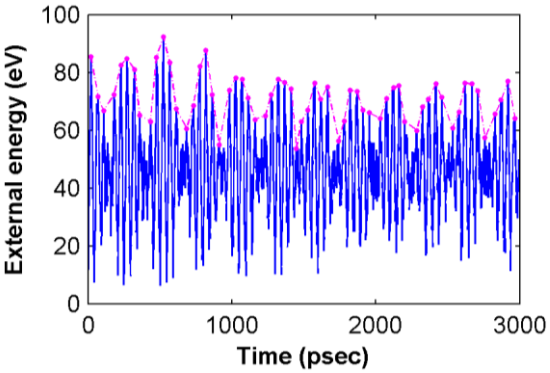

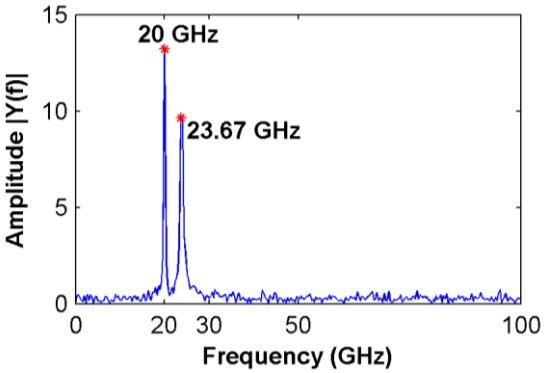

2.9 Group IX: 8 cases. Consider different actuation directions

Setting: Circular Ag NWs; Size: 6×34.71 nm^2; Temp.: 10 K; Vel.: 0.8 Å/psec.

2.9.1 Coordination system C1, actuation in x-axis

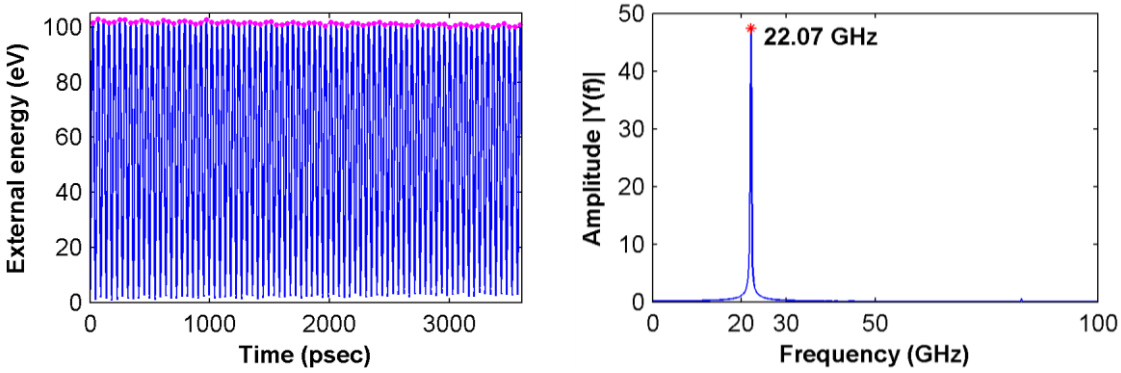

2.9.2 Coordination system C1, actuation in y-axis

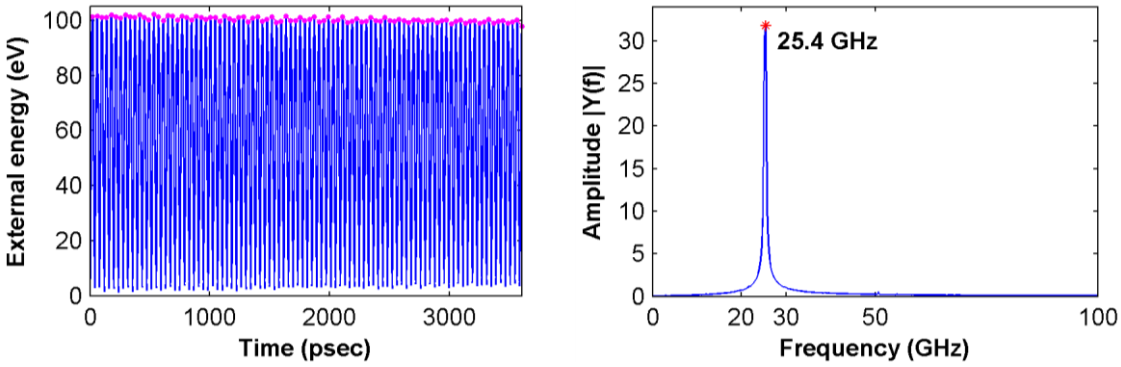

2.9.3 Coordination system C2, actuation in x-axis

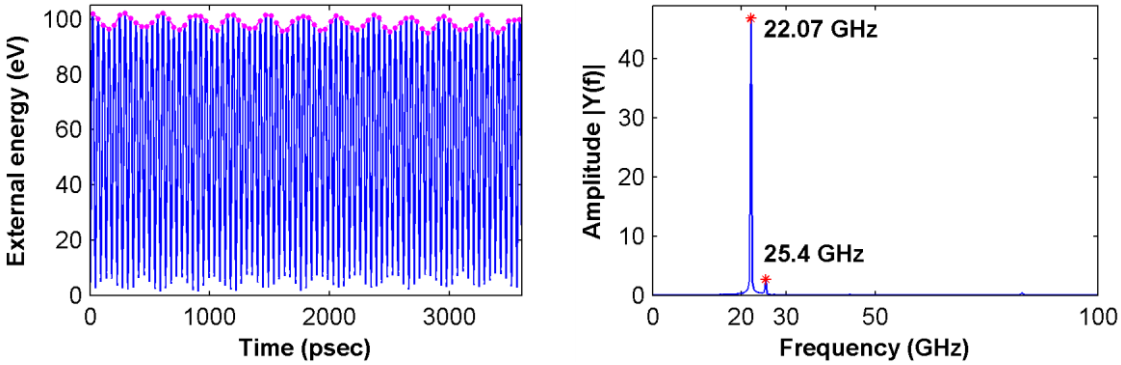

2.9.4 Coordination system C2, actuation in y-axis

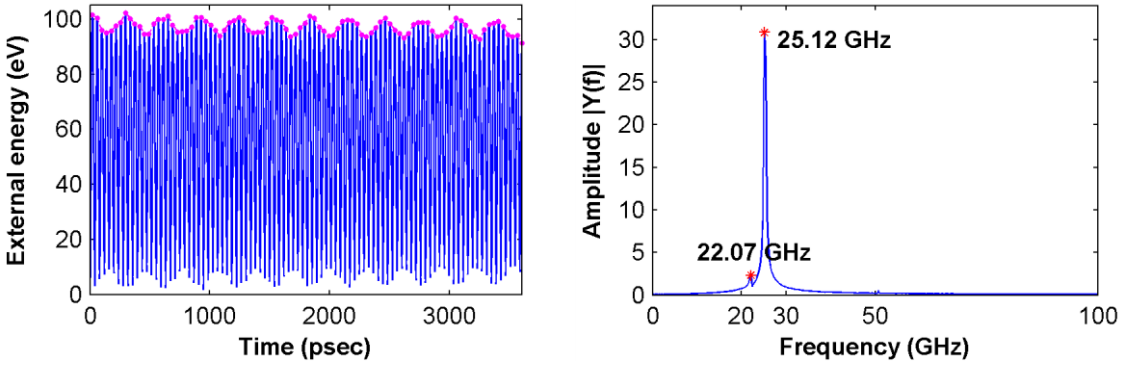

2.9.5 Coordination system C3, actuation in x-axis

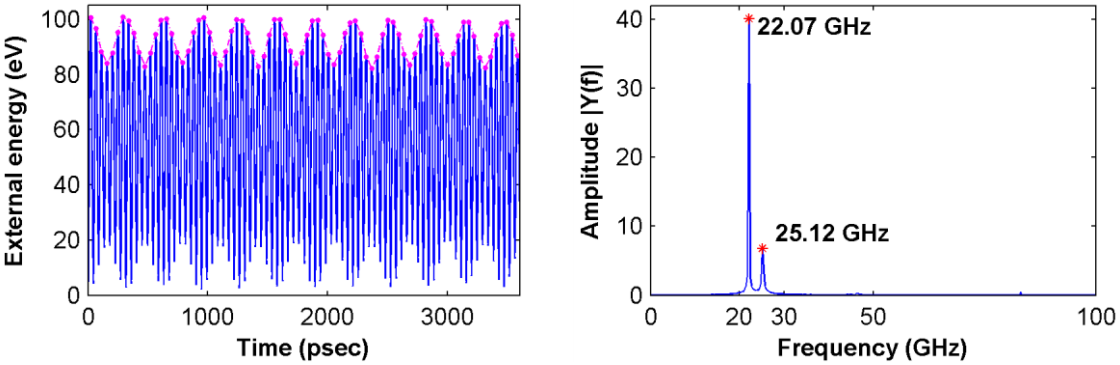

2.9.6 Coordination system C3, actuation in y-axis

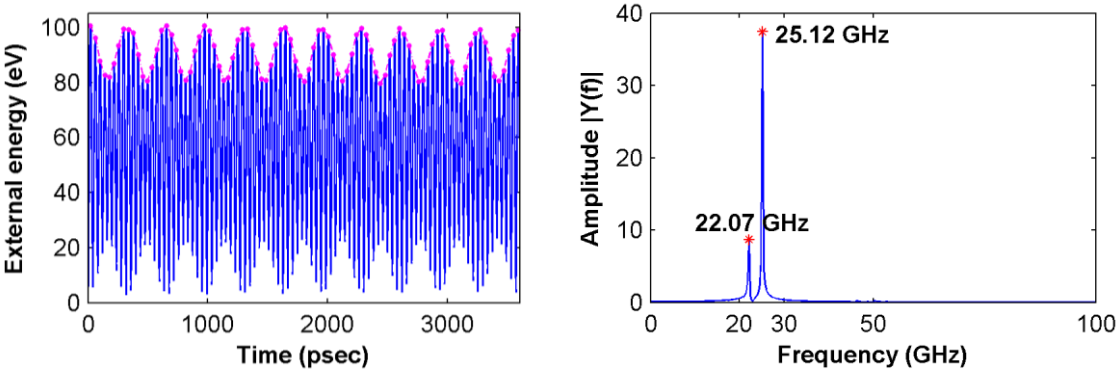

2.9.7 Coordination system C4, actuation in x-axis

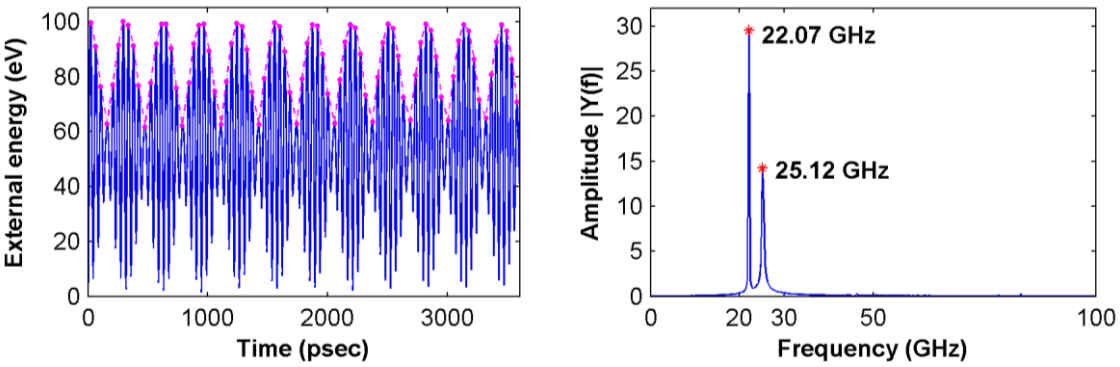

2.9.8 Coordination system C4, actuation in y-axis

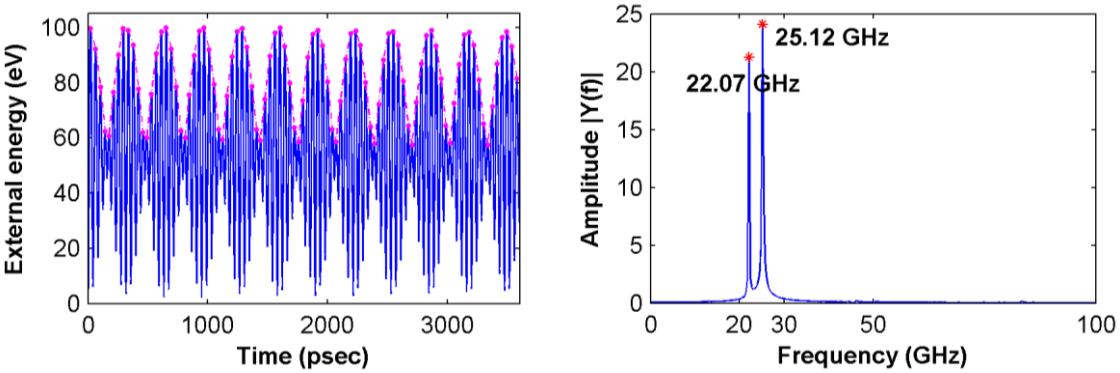

2.10 Group X: 12 cases. Consider different cross-sectional geometries

Setting: Ag NWs; Temp.: 10 K; Initial Coord. (*x* and *y*-axes): C1; Velocity actuation

The schematics of three different kinds of cross-sections are shown in Fig. 1, together with the four specific actuation directions for each case.

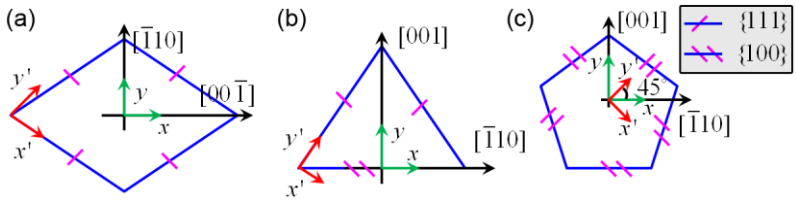

Fig. 1.(a) The rhombic cross-section. (b) The triangular cross-section. (c) The pentagonal cross-section.

2.10.1 Rhombic cross-section, actuation in x-axis, 0.4 Å/psec

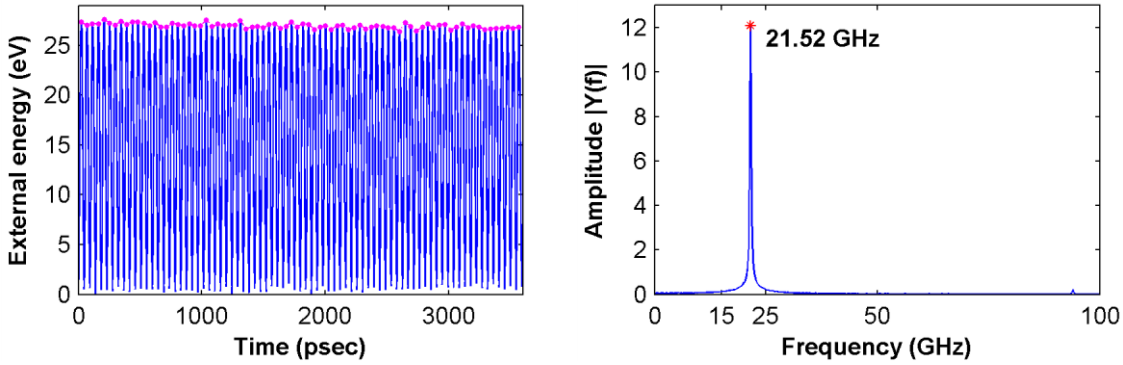

2.10.2 Rhombic cross-section, actuation in y-axis, 0.4 Å/psec

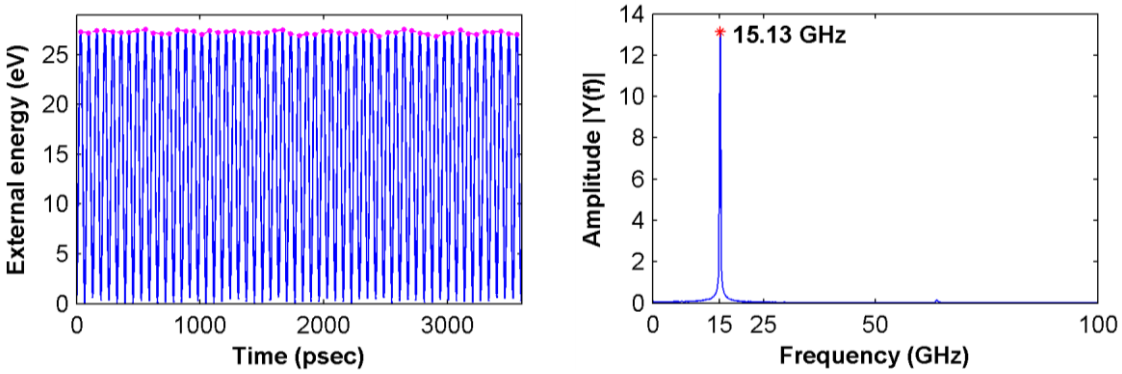

2.10.3 Rhombic cross-section, actuation in x'-axis, 0.4 Å/psec

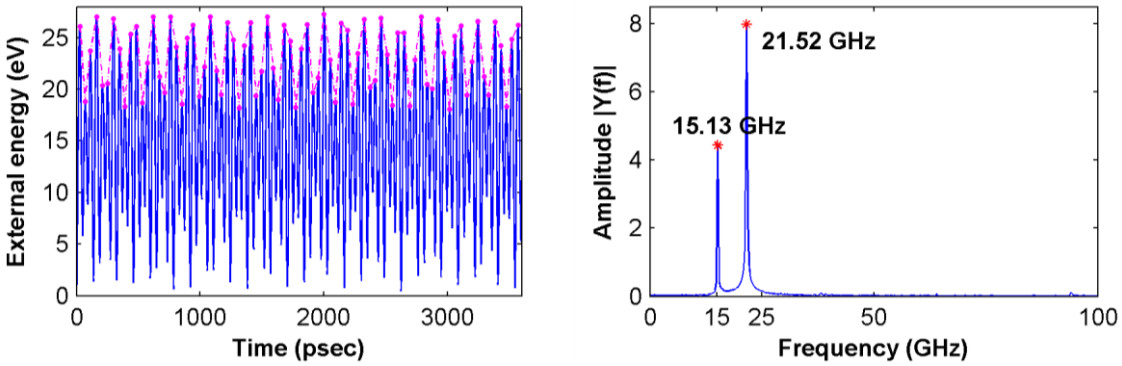

2.10.4 Rhombic cross-section, actuation in y'-axis, 0.4 Å/psec

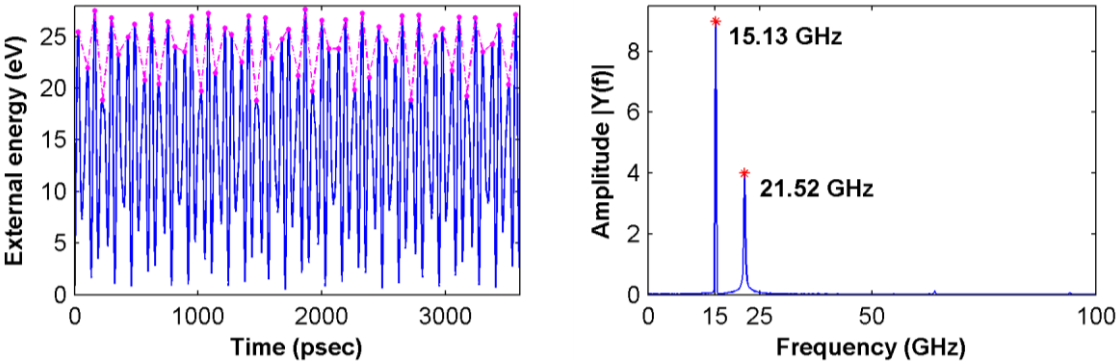

2.10.5 Triangular cross-section, actuation in x-axis, 0.2 Å/psec

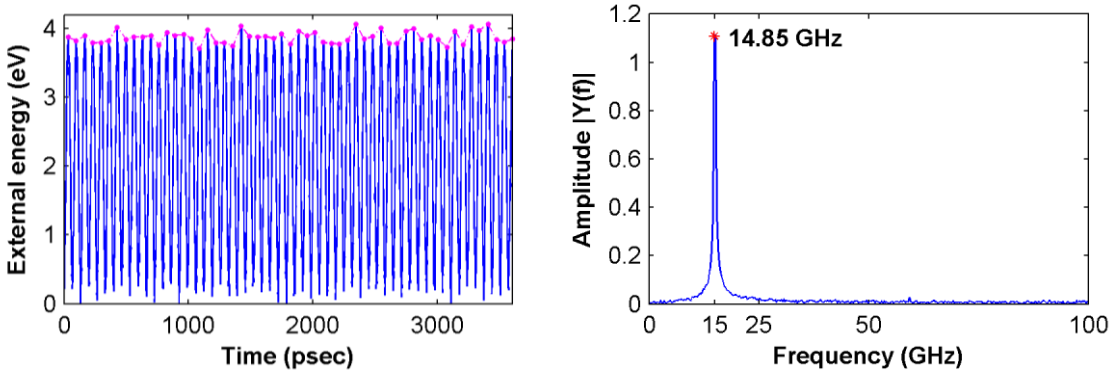

2.10.6 Triangular cross-section, actuation in y-axis, 0.2 Å/psec

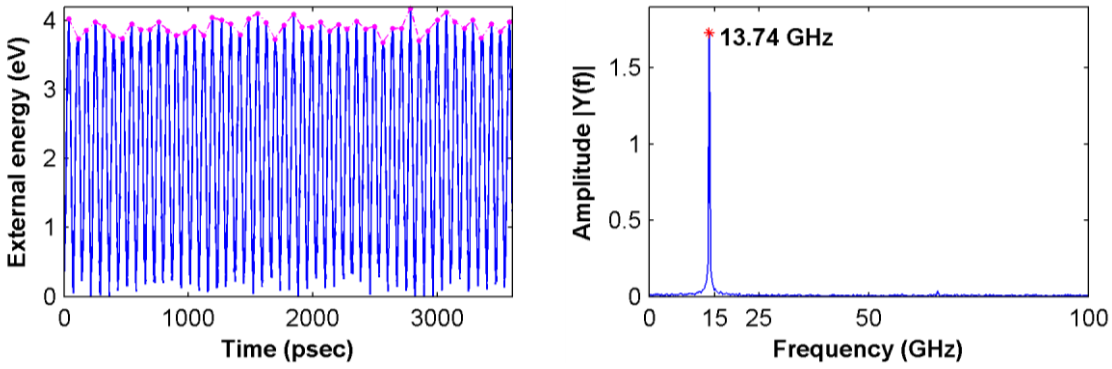

2.10.7 Triangular cross-section, actuation in x'-axis, 0.2 Å/psec

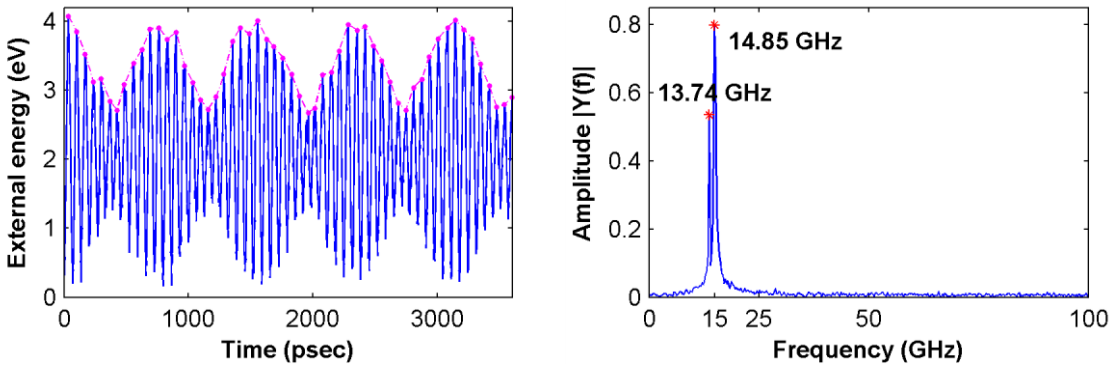

2.10.8 Triangular cross-section, actuation in y'-axis, 0.2 Å/psec

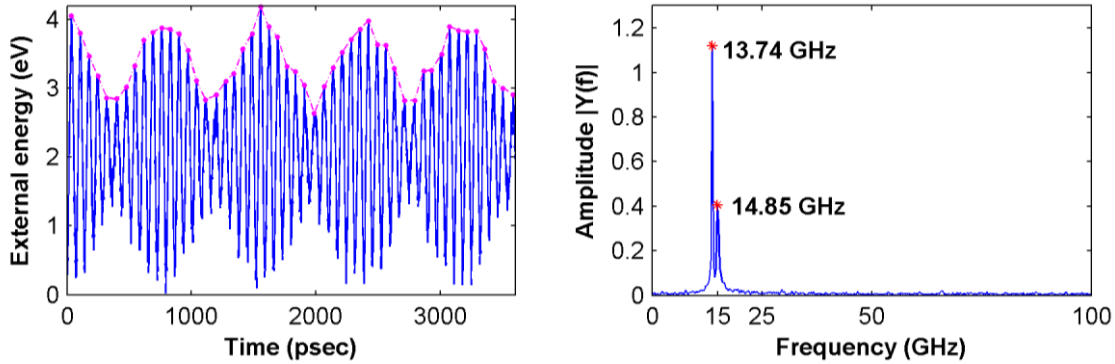

2.10.9 Au NW, pentagonal cross-section, actuation in x-axis, 0.5 Å/psec

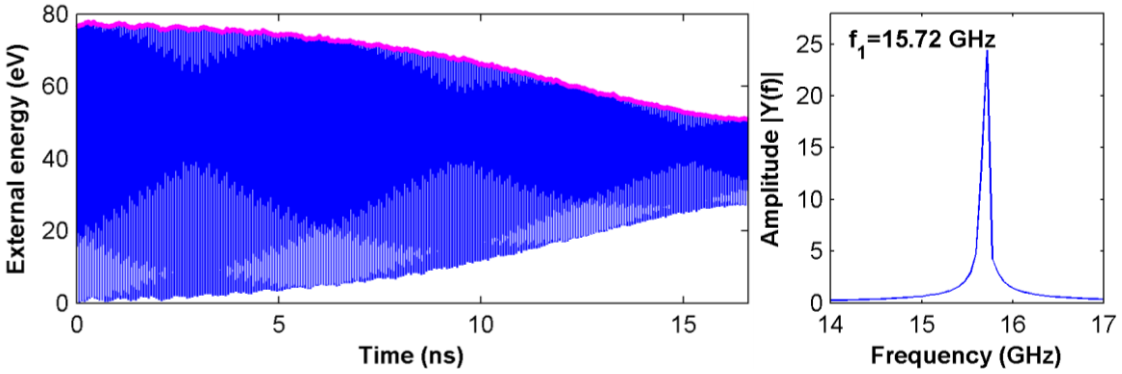

2.10.10 Au NW, pentagonal cross-section, actuation in y-axis, 0.5 Å/psec

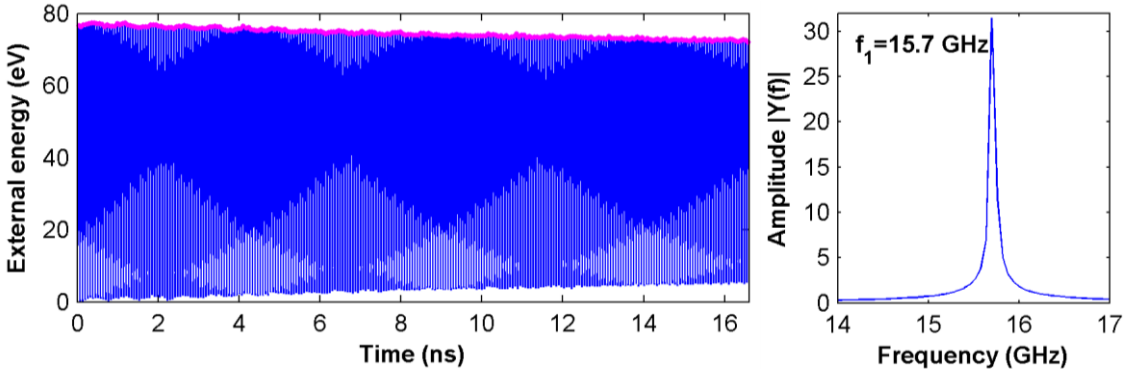

2.10.11 Au NW, pentagonal cross-section, actuation in x'-axis, 0.5 Å/psec

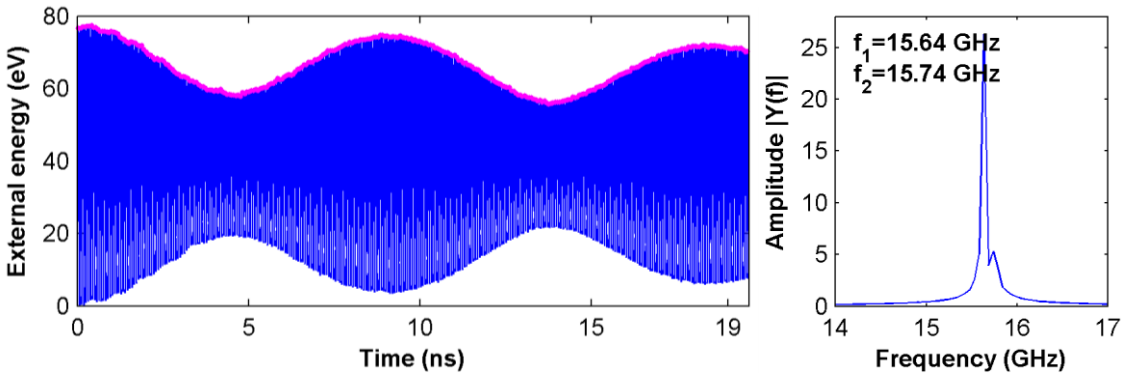

2.10.12 Au NW, pentagonal cross-section, actuation in y'-axis, 0.5 Å/psec

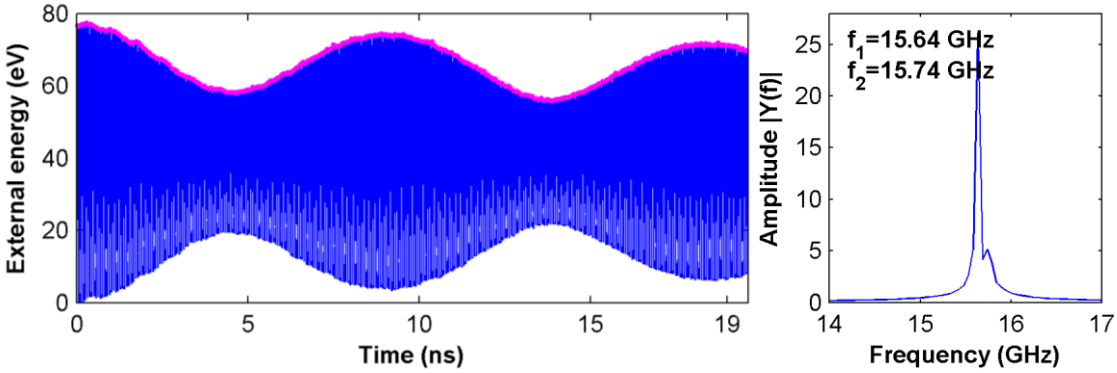

2.11 Group XI: 1 case. Consider simultaneous actuations in both *x* and *y*-axes

Setting: Circular Ag NWs; Size: 6×34.71 nm^2; Coord.: C0; Temp.: 10 K; Simultaneous Vel.: *x*-axis: 0.46188 Å/psec & *y*-axis: -0.6532 Å/psec

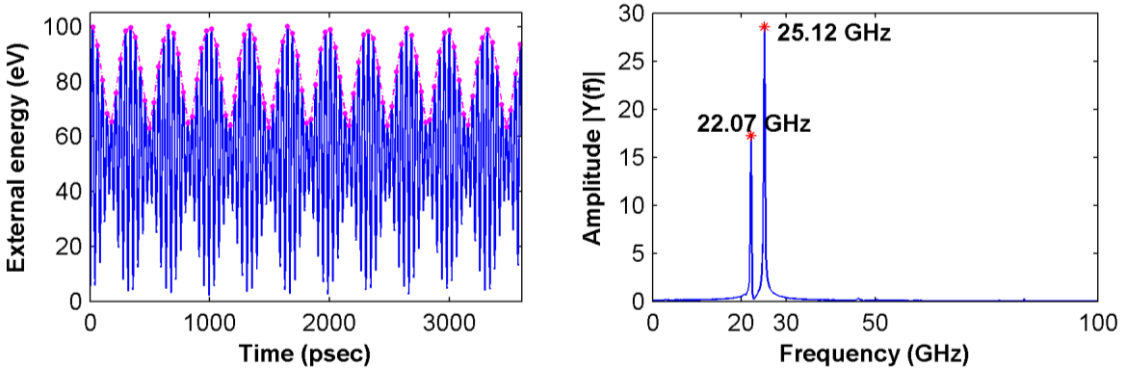

2.12 Group XII: 5 cases. Consider other [110] orientated FCC NWs

Setting: Circular cross-section; Coord.: C0; Temp.: 10 K; Vel.: *x*-axis.

EAM potentials developed by Foiles et al.[1] are employed to describe the atomic interactions between the Cu, Au, Ni, Pd, and Pt atoms.

2.12.1 Cu NW, Size: 6×34.76 nm^2, Vel.: 0.8 Å/psec

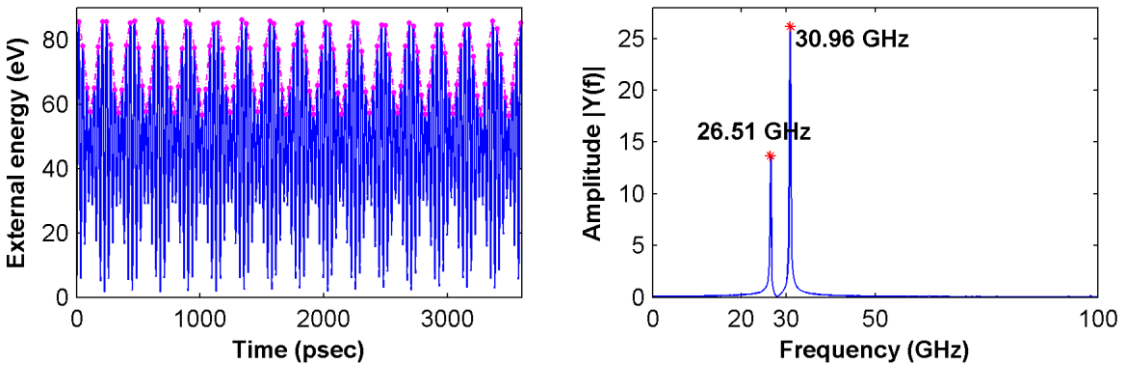

2.12.2 Au NW, Size: 6×34.62 nm^2, Vel.: 0.4 Å/psec

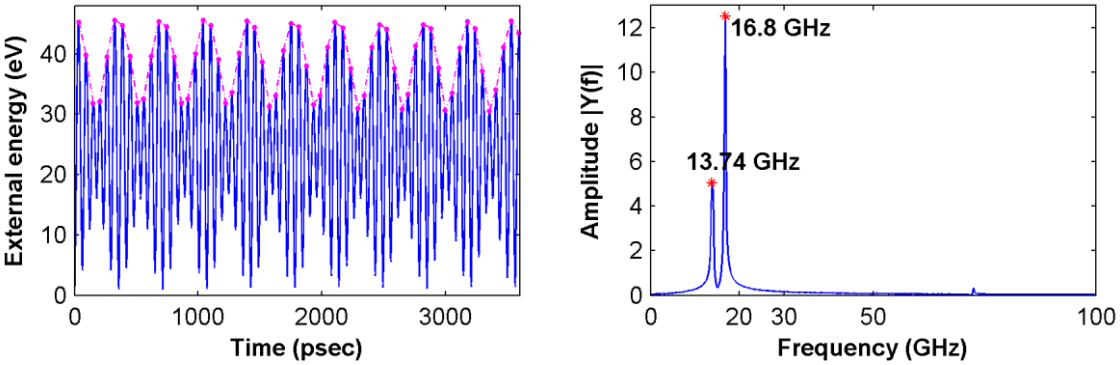

2.12.3 Ni NW, Size: 6×34.85 nm^2, Vel.: 0.8 Å/psec

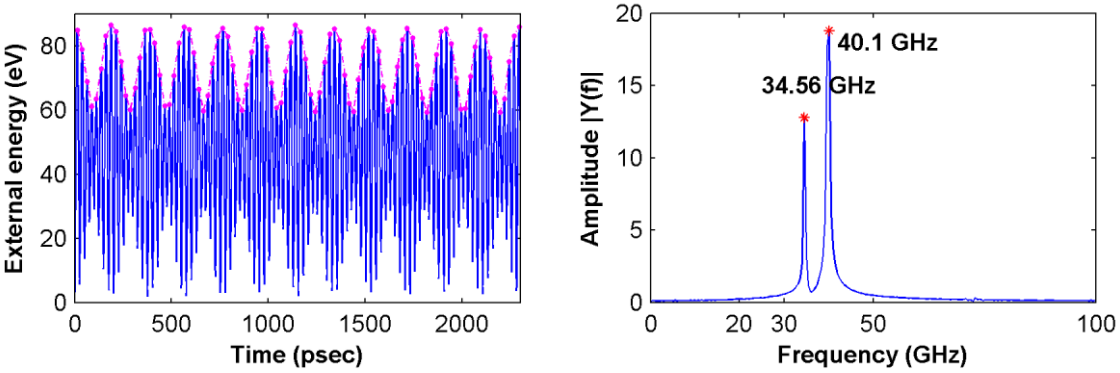

2.12.4 Pt NW, Size: 6×34.37 nm^2, Vel.: 0.3 Å/psec

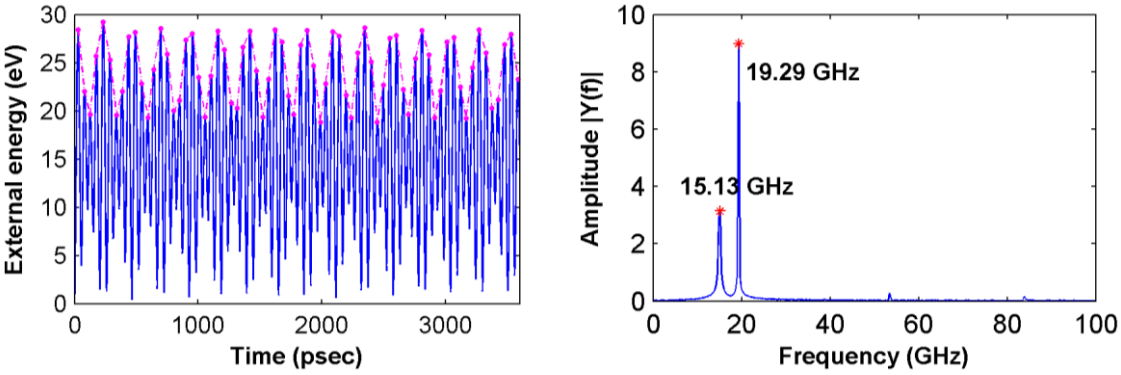

2.12.5 Pd NW, Size: 6×34.66 nm^2, Vel.: 0.8 Å/psec

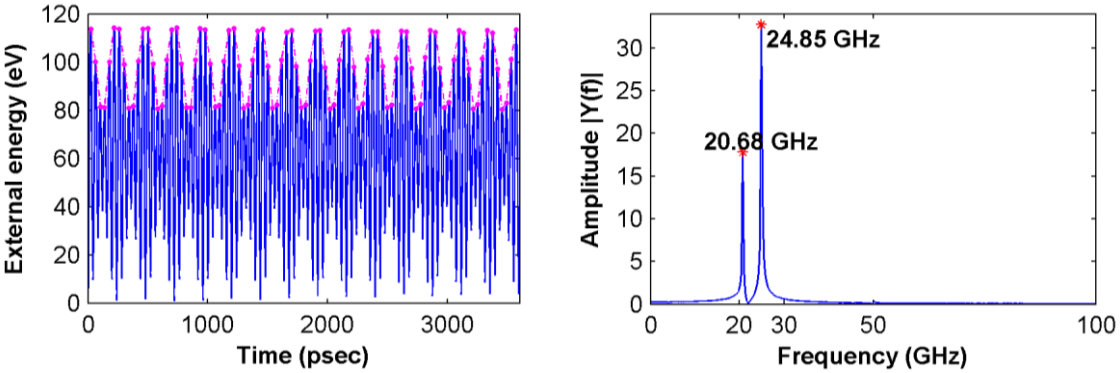

2.13 Group XIII: 10 cases. Consider different square cross-sectional sizes

Setting: Square Ag NW; Coord.: C1; Temp.: 10 K; Simultaneous velocity actuations in *x and y*-axes.

2.13.1 Size: b=3.27 nm, L=32.97 nm

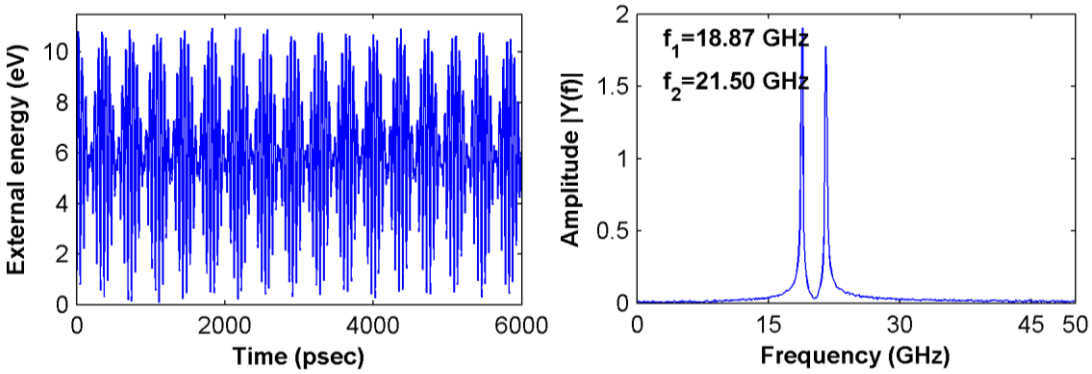

2.13.2 Size: b=4.09 nm, L=41.65 nm

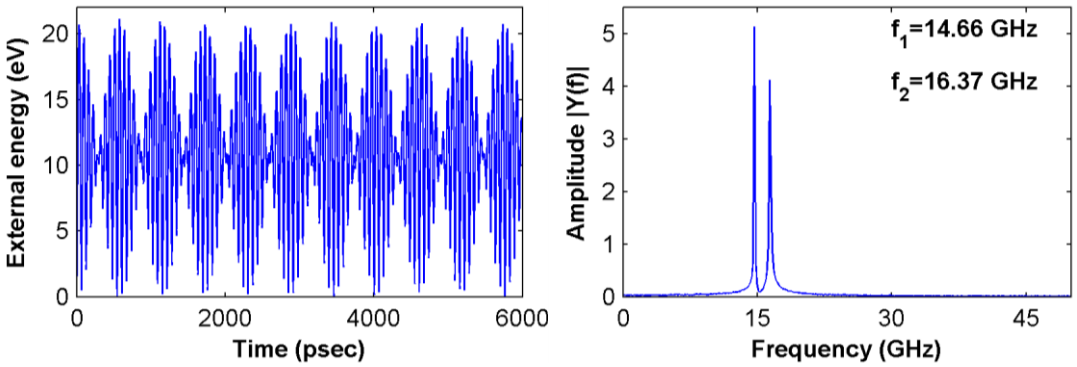

2.13.3 Size: b=4.34 nm, L=44.54 nm

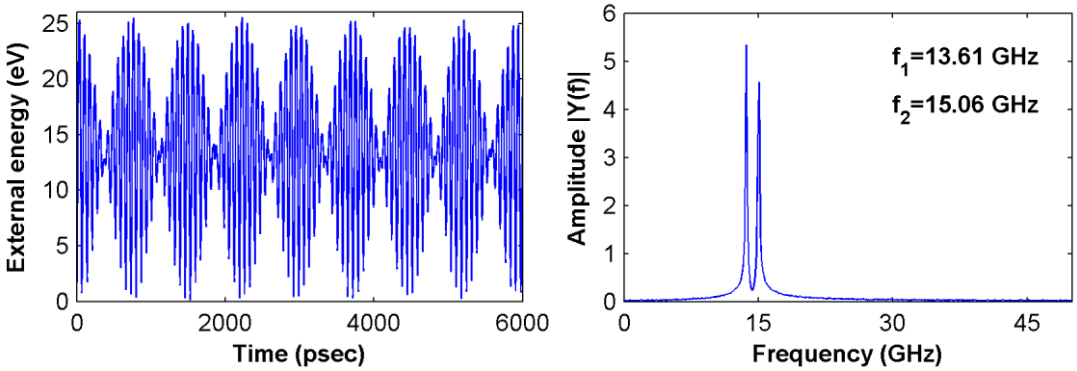

2.13.4 Size: b=4.92 nm, L=50.32 nm

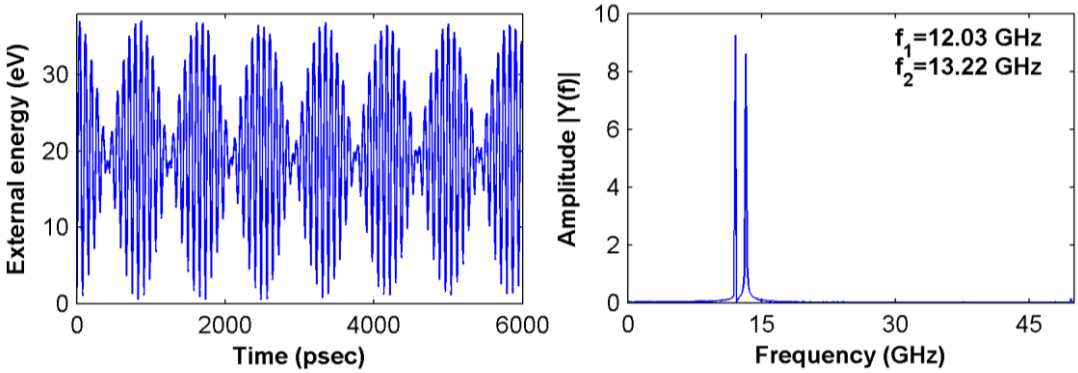

2.13.5 Size: b=5.32 nm, L=53.21 nm

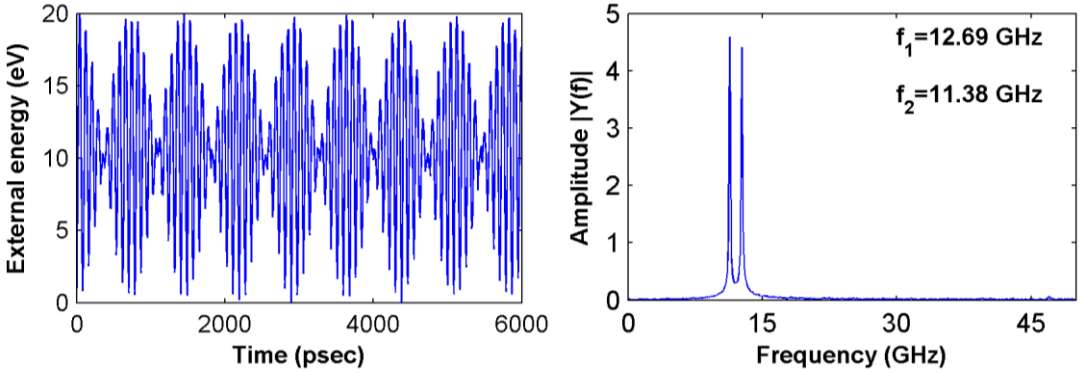

2.13.6 Size: b=5.78 nm, L=59.00 nm

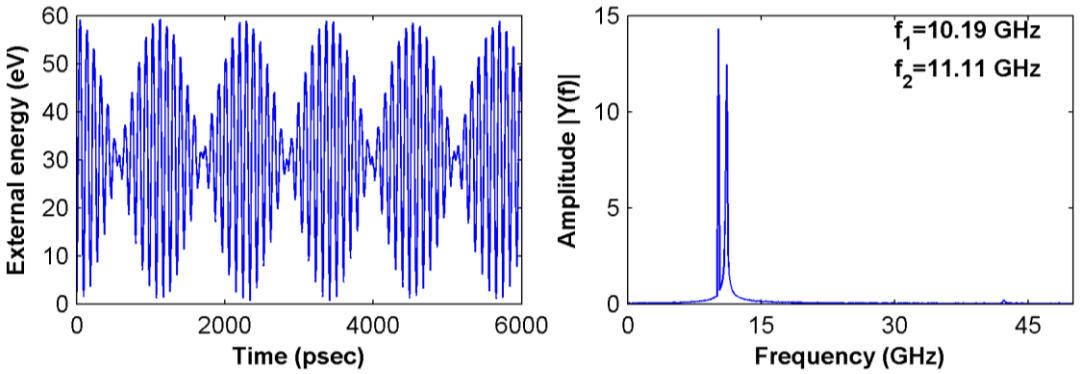

2.13.7 Size: b=6.14 nm, L=61.89 nm

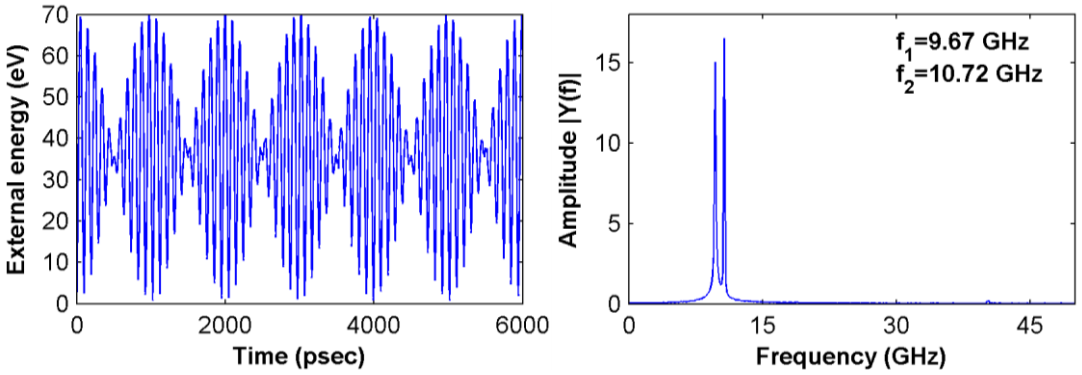

2.13.8 Size: b=6.36 nm, L=64.78 nm

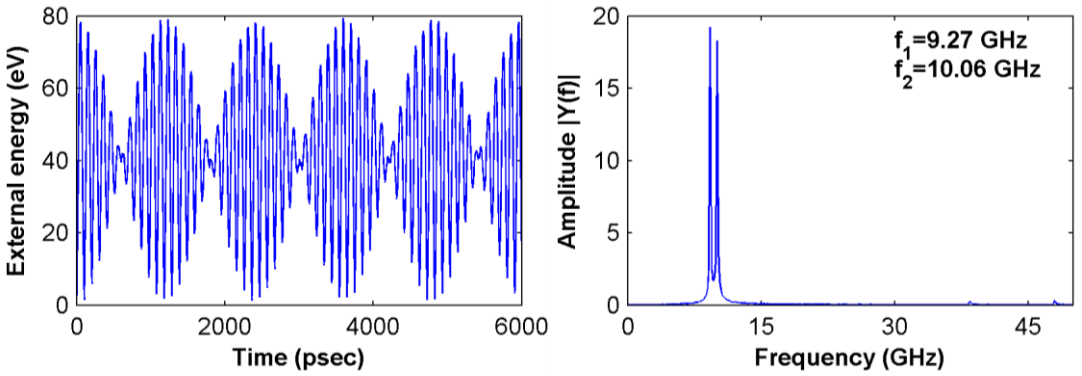

2.13.9 Size: b=6.95 nm, L=70.57 nm

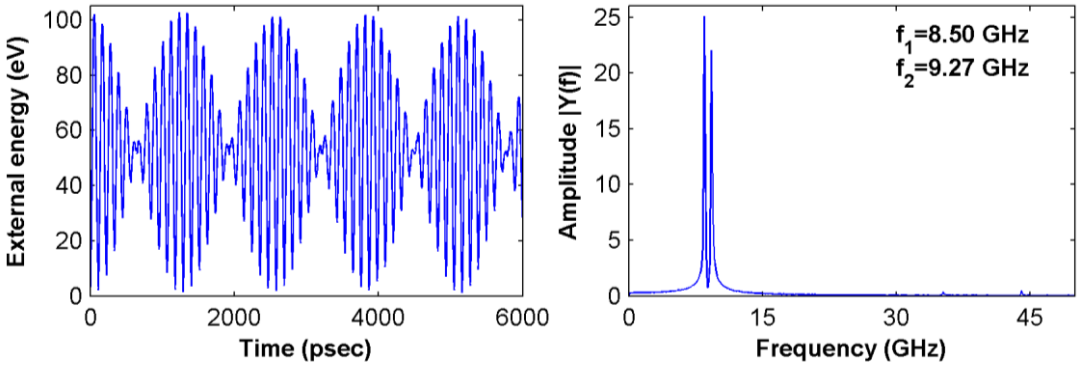

2.13.10 Size: b=7.81 nm, L=79.24 nm

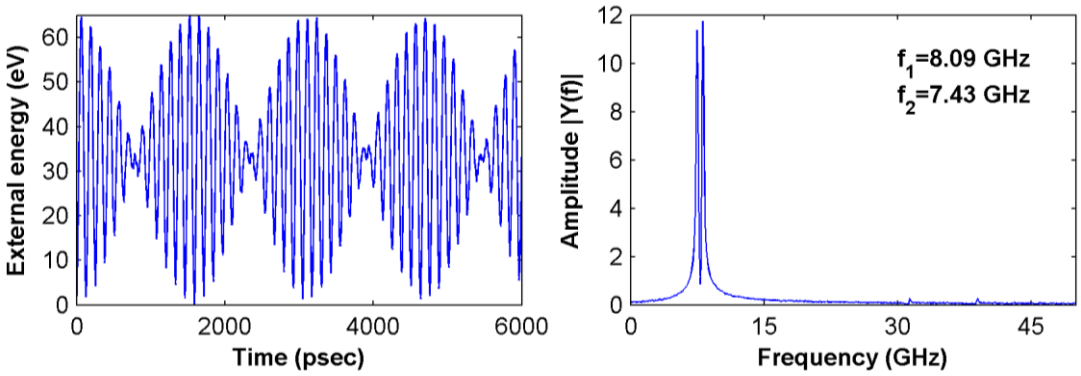

3 Derivation Details

3.1 Estimation of the effective flexural rigidity

Estimation of the effective flexural rigidity is conducted for a nearly square cross-section. For the FCC crystal structure, the [110] orientated NW could be taken as constructed by repeating two adjacent (110) atomic layers in the longitudinal direction. Particular, these two atomic layers possess identical atomic arrangement. Hence, a single (110) layer is taken as a fundamental element for the calculation of the effective flexural rigidity. Following figure shows a snapshot of a {110} atomic layer.

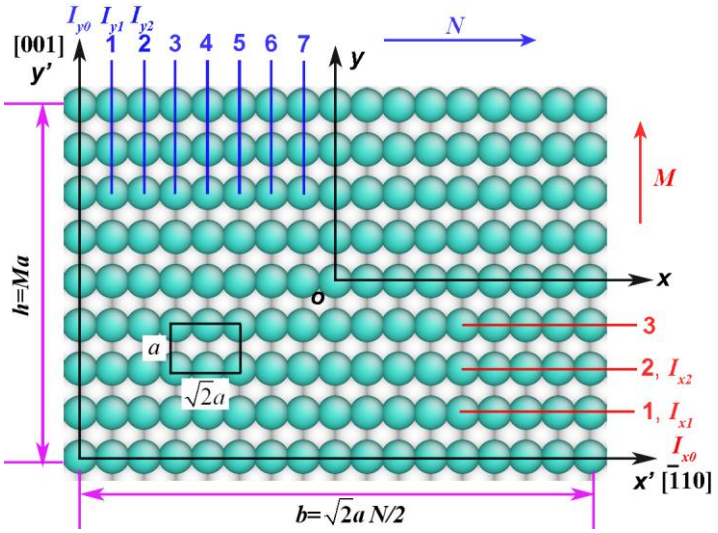

Fig. 2. A snapshot of a {110} atomic layer. Grey atoms represent the adjacent lower layer.

Basing on the composite beam theory,[2] the effective flexural rigidity is given as (with the consideration of the surface effect):[3]

$$\begin{cases}(EI)_x^* = EI_x + E_{s1}bh^2/2 + E_{s2}h^3/6 \\ (EI)_y^* = EI_y + E_{s2}hb^2/2 + E_{s1}b^3/6\end{cases} \quad (1)$$

where E is the bulk Young's modulus, E_{s1} and E_{s2} are the {100} and {110} surface Young's modulus, respectively. Considering the fact that the atomic system is discrete in nature, which means the moment of inertia could be mathematically expressed as

$$\begin{cases}I_x = \int_A y^2 dA = \sum\left(y_n^2 A_n + I_a\right) \\ I_y = \int_A x^2 dA = \sum\left(x_n^2 A_n + I_a\right)\end{cases} \quad (2)$$

where A_n is the atom's projection area ($A_n = \pi r^2$, and r is the atom radius), x_n and y_n are the coordinates of the atom, I_a is the moment of inertia for a single atom along its own symmetry axis ($I_a = \pi r^4/4$). Consider each atom as a hard sphere, the atom radius could be expressed as $r = a/(2\sqrt{2})$, where a is the lattice constant. Hence, the effective flexural rigidity could be derived as below:

1) For the moment of inertia along the *x*-axis

We have $I_x = I_{x'} - A(h/2)^2 = \sum\left(y_n^2 A_a + I_a\right) - Ah^2/4$

From Fig. 2, the column numbers of atoms are designated as N and M in the x and y-axes, respectively, i.e., $b = \sqrt{2}aN/2$, $h = Ma$. Therefore, the moment of inertia along the *x'*-axis could be expressed as $I_{x'} = I_{x0} + I_{xm}$, where

$I_{x0} = (N+1)I_a$, $I_{xm} = I_{x1} + I_{x2} + ... + I_{xi} + ... + I_{xM}$, and $I_{xi} = (N+1)\left[A_a(ia)^2 + I_a\right]$. Hence,

$I_{xm} = (N+1)\left(A_a a^2 \sum_{i=1}^{M} i^2 + MI_a \right)$. Thus,

$I_{x'} = (M+1)(N+1)I_a + A_a a^2 (N+1)M(M+1)(2M+1)/6$, $A = (M+1)(N+1)A_a$

$I_x = (M+1)(N+1)I_a + A_a a^2 (N+1)M(M+1)(2M+1)/6 - A_a a^2 M^2 (M+1)(N+1)/4$

2) For the moment of inertia along the *y*-axis

As $I_y = I_{y'} - A(b/2)^2 = \sum\left(x_n^2 A_a + I_a \right) - Ab^2/4$

From Fig. 2, $I_{y'} = I_{y0} + I_{yn}$, where

$I_{y0} = (M+1)I_a$, $I_{yn} = I_{y1} + I_{y2} + ... + I_{yi} + ... + I_{yN}$, and $I_{yi} = (M+1)\left[A_a \left(ia\sqrt{2}/2 \right)^2 + I_a \right]$. Hence,

$I_{yn} = (M+1)\left(\frac{1}{2} A_a a^2 \sum_{i=1}^{N} i^2 + NI_a \right)$. Thus,

$I_{y'} = (M+1)(N+1)I_a + A_a a^2 (M+1)N(N+1)(2N+1)/12$

$I_y = (M+1)(N+1)I_a + A_a a^2 (M+1)N(N+1)(2N+1)/12 - A_a a^2 N^2 (M+1)(N+1)/8$

Therefore, the effective flexural rigidity $(EI)_x^*$ and $(EI)_y^*$ (include the surface effect) can be obtained. From the classical Euler-Bernoulli beam theory,[4] the resonance frequency of a thin NW is expressed as

$$f = \frac{\omega_n}{2\pi L^2}\sqrt{\frac{(EI)}{\rho A}}$$

where ρ is the density, A is the cross-sectional area of the NW and ω_n is the eigenvalue corresponding to different boundary conditions. Therefore, due to the two different principal moments of inertia, two frequencies are obtained, and their relationship follows:

$$\frac{f_y}{f_x} = \sqrt{\frac{(EI)_x^*}{(EI)_y^*}}$$

Where f_x and f_y are the frequencies in the *x* and *y*-axes (i.e., $[\bar{1}10]$ and [001] directions), respectively. Recall Fig. 2, let $h \approx b$ to consider a nearly square cross-section, then the difference between the two frequency components can be estimated.

3.2 Relation of the spring elastic constant and beam elastic modulus

Consider a spring with the elastic constant of *k*, and a beam with the length of *L*, the cross-sectional area of *A* and elastic modulus of *E*. Then the displacements of them subjecting to a force *F* can be described as below:

For the spring, $\Delta x_s = \frac{F}{k}$

For the beam, $\Delta x_b = \frac{FL}{EA}$

According to the Cauchy law, the spring is equivalent to a beam in the elastic regime, that is $\Delta x_s = \Delta x_b$. Hence, $\frac{F}{k} = \frac{FL}{EA}$, means, $k = \frac{EA}{L}$.

Recall the simplified spring-mass system for the NW in Fig. 1d in the manuscript, and assume the equivalent beams for spring k_1 and k_2 have identical length and cross-sectional size, we then have:

$\frac{k_1}{k_2} = \frac{E_1}{E_2}$.

3.3 Slightly damped mass-spring system under harmonic force

The NW is simplified as a damped mass-spring system in each elementary direction. The force $F = F_0 \sin(\omega t)$ represents the harmonic excitation exerted by the AC electric field. According to the vibration theory,[4] the governing equation in the *x*-axis could be written as:

$M\ddot{x} - k_1 x - c\dot{x} = F_1 \sin(\omega t)$

where $F_1 = F_0 \cos\theta$. The solution for the above equation is constituted by two parts as: $x = x_1 + x_2$. In particular, x_1 is the solution to an undamped oscillation $x_1 = A_x e^{-nt} \sin\left(\sqrt{(\omega_{n1}^2 - n^2)}t + \alpha_x\right)$ (for $n < \omega_{n1}$), where A_x is the amplitude, α_x is the phase lag angle, $\omega_{n1}^2 = k_1 / M$ and $2n = c / M$. x_2 is a stable oscillation, which takes the form of $x_2 = B_x \sin(\omega t - \varphi_x)$, here B_x is the amplitude and φ_x is the phase lag of the vibration against the sinusoidal force. Substitute x_2 to the governing equation, we obtain

$$B_x = \frac{F_1}{M\sqrt{(\omega_{n1}^2 - \omega^2)^2 + 4n^2\omega^2}}$$

$$\varphi_x = tg^{-1}\frac{2n\omega}{\omega_{n1}^2 - \omega^2}$$

Therefore, the solution to the governing equation is

$$x = A_x e^{-nt} \sin\left(\sqrt{(\omega_{n1}^2 - n^2)}t + \alpha_x\right) + B_x \sin(\omega t - \varphi_x)$$

The first term in the left hand of the above solution decays with time, which is usually short-lived and can be ignored, hence, only the second term is considered. Let $h_1 = F_0 / k_1$, $\zeta_1 = n / \omega_{n1}$ and $\lambda_1 = \omega / \omega_{n1}$, then the amplitude could be expressed as

$$B_x = \frac{h_1 \cos\theta}{\sqrt{(1-\lambda_1^2)^2 + 4\zeta_1^2\lambda_1^2}}$$

Following the same procedure, with a same damping factor and considering the force in the *y*-axis as $F_y = F\sin\theta$, the amplitude in the *y*-axis could be expressed as

$$B_y = \frac{h_2 \sin\theta}{\sqrt{(1-\lambda_2^2)^2 + 4\zeta_2^2\lambda_2^2}}$$

where $h_2 = F_0 / k_2$, $\zeta_2 = n/\omega_{n2}$, $\lambda_2 = \omega/\omega_{n2}$ and $\omega_{n2}^2 = k_2/M$. According the linear superposition principal, the amplitude in the excitation direction is $B_{xy} = B_x\cos\theta + B_y\sin\theta$. Let $\beta_{xy} = B_{xy}k_2/F_0$, hence,

$$\beta_{xy} = \beta_x\cos\theta + \beta_y\sin\theta = \frac{\cos^2\theta}{\sqrt{(r-\lambda^2)^2 + 4\zeta^2\lambda^2}} + \frac{\sin^2\theta}{\sqrt{(1-\lambda^2)^2 + 4\zeta^2\lambda^2}}$$

where $r = k_1/k_2$, $\lambda = \lambda_2$ and $\zeta = \zeta_2$. Using the condition $d\beta_x/d\lambda = 0$ and $d\beta_y/d\lambda = 0$, the resonant frequency of a forced vibration is at

$$\begin{cases} \lambda_{r1} = \sqrt{r - 2\zeta^2} \\ \lambda_{r2} = \sqrt{1 - 2\zeta^2} \end{cases}$$

The corresponding amplitude reaches a maximum value of

$$\begin{cases} \beta_{r1} = \dfrac{\cos^2\theta}{2\zeta\sqrt{r-\zeta^2}} + \dfrac{\sin^2\theta}{\sqrt{(1-r)^2 + 4\zeta^2 - 4\zeta^4}} \\ \beta_{r2} = \dfrac{\cos^2\theta}{\sqrt{(r-1)^2 + 4r\zeta^2 - 4\zeta^4}} + \dfrac{\sin^2\theta}{2\zeta\sqrt{1-\zeta^2}} \end{cases}$$

Consider the Ag NW studied in this work, according to Sec. 3.2, we have $r = E_1/E_2 = 67.23/87.09 \approx 0.77$. Figure 3 shows the relative amplitude as a function of both the excitation angle and the damping ratio. Evidently, the increase of damping ratio reduces the difference between the relative magnitudes at the two resonance frequencies. Particularly, in Fig. 3d, only one peak value is observed when the excitation angle varies from 0 to 90°, which means, under such a damping condition, only one frequency component can be resolved from the resonance experiments.

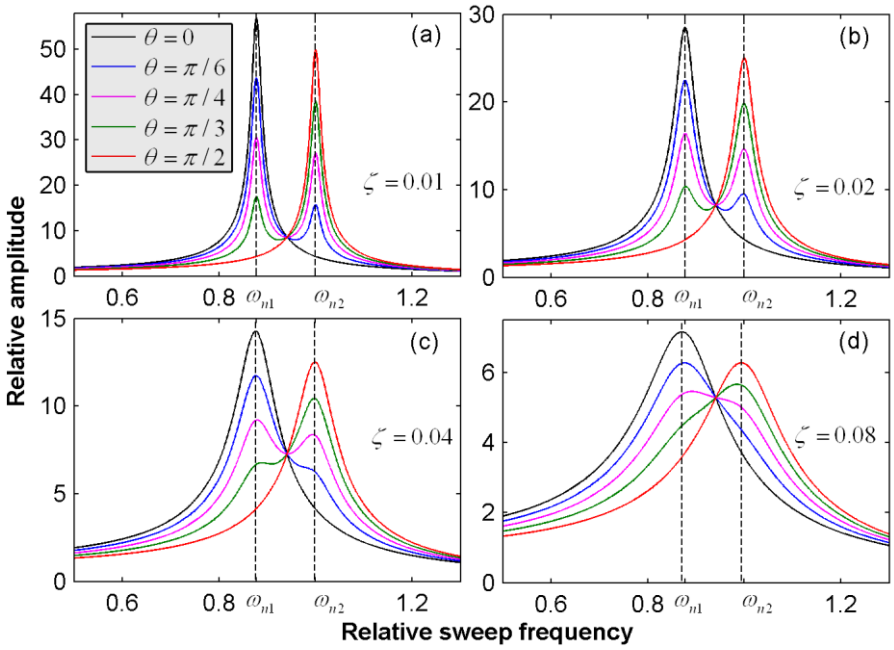

Fig. 3. The relative amplitude as a function of the excitation angle and the damping ratio. (a) Damping ratio of 0.01; (b) Damping ratio of 0.02; (c) Damping ratio of 0.04; (d) Damping ratio of 0.08.

Let $\Delta\beta = |\beta_{r1} - \beta_{r2}|$, from Fig. 4a, it is apparent that difference between the relative amplitudes at the two resonance frequencies varies when the excitation angle changes from 0 to 90°. As Fig. 3 has discussed a relative large damping ratio, here we discuss when the damping ratio is very small. Consider that, the damping ratio is directly related with the quality (Q) factor as $Q = 1/\left(2\zeta\sqrt{1-\zeta^2}\right)$.[5] From the MD results on metal NWs,[6] let Q-factor equals 5000, which indicates a damping ratio of $\zeta = 1e-4$. To make quantitative analysis, we assume that, the resonance frequency with smaller amplitude is detectable only when its value satisfy $\beta_{\min} \geq \eta\beta_{\max}$, here η indicates the confidential level. This means, to detect both resonance frequencies, $\Delta\beta / \beta_{\max} \leq 1-\eta$. Figure 4b presents the value of $\Delta\beta / \beta_{\max}$ as a function of both damping ratio ζ and the excitation angle θ (when $\eta = 0.3$). As is seen, the confidential interval Ω with both resonance frequencies detectable increase with the increase of the damping ratio. Define the probability as $P = \Omega / (\pi / 2)$, this means P decreases with the decrease of damping ratio. For the current Ag NW with $r = 0.77$ and $Q = 5000$, P is estimated around 0.36. This result indicates a much larger propensity to detect one single resonance frequency rather than both of them for the relatively small damping ratio.

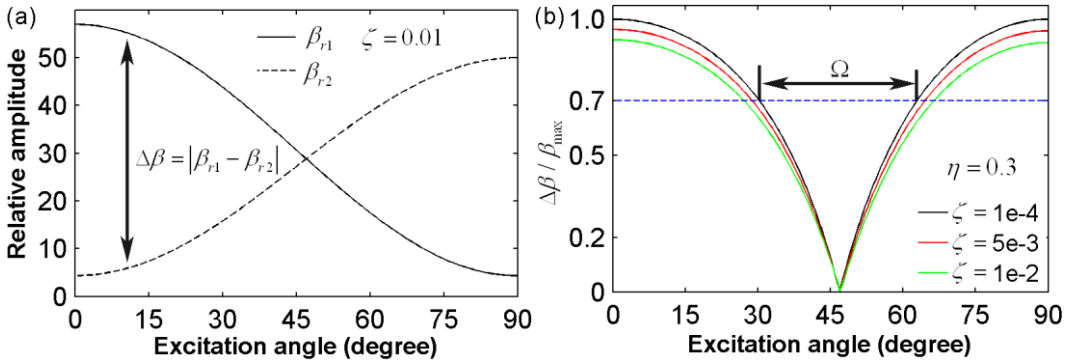

Fig. 4. (a) The relative amplitudes at two resonance frequencies as a function of the excitation angle. (b) The value of $\Delta\beta / \beta_{\max}$ as a function of both damping ratio ζ and the excitation angle θ (when $\eta = 0.3$).

It is interesting to consider the critical excitation angle θ_{cr} when $\beta_{r1} = \beta_{r2}$, which is obtained as:

$$\theta_{cr} = \arctan\left(\sqrt{\frac{\frac{1}{2\zeta\sqrt{r-\zeta^2}} - \frac{1}{\sqrt{(r-1)^2 + 4r\zeta^2 - 4\zeta^4}}}{\frac{1}{2\zeta\sqrt{1-\zeta^2}} - \frac{1}{\sqrt{(1-r)^2 + 4\zeta^2 - 4\zeta^4}}}}\right)$$

According to the above derivation, the critical excitation angle is a function of the damping ratio ζ and the ratio r between the two values of Young's modulus. As shown in Fig. 5, the critical angle increases with the increase of ζ and the decrease of r. This fact means a larger domain of $\beta_{r1} \geq \beta_{r2}$ for larger ζ or smaller r. In other words, by taking the resonance frequency with larger amplitude as the NW's natural frequency will most likely yield to the smaller frequency components, and thus the smaller Young's modulus.

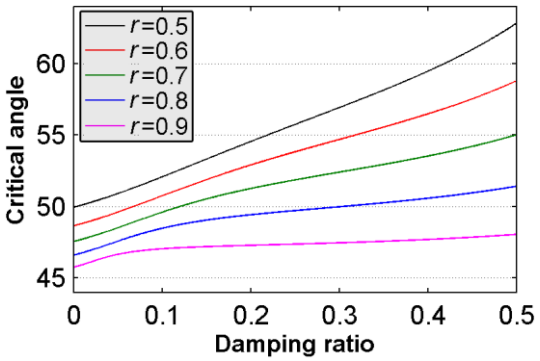

Fig. 5. The critical excitation angle as a function of the damping ratio and the ratio of the two values of Young's modulus.

REFERENCES

1. S. M. Foiles, M. I. Baskes and M. S. Daw, Phys. Rev. B **33** (12), 7983-7991 (1986).
2. J. Gere and S. Timoshenko, *Mechanics of Materials*, 4th ed. (Cheltenham, UK: Stanley Thornes, 1999).
3. J. He and C. M. Lilley, Nano Lett. **8** (7), 1798-1802 (2008).
4. S. G. Kelly, *Advanced vibration analysis*. (CRC Press, 2007).
5. M. H. Bao, *Analysis and design principles of MEMS devices*. (Elsevier Science, 2005).
6. S. Y. Kim and H. S. Park, Phys. Rev. Lett. **101** (21), 215502 (2008).